Systematic Review Article
http://mjiri.iums.ac.ir
Medical Journal of the Islamic Republic of Iran (MJIRI)

Med J Islam Repub Iran. 2025 (8 Jul);39.91. https://doi.org/10.47176/mjiri.39.91

The Application of Magnetic Particles for Cell Targeting in Preclinical Animal Models: A Systematic Review

Viktor Turchin[1]*, Roman Ishchenko[1], Svetlana Bespalova[2], Maxim Solopov[1], Mikhail Kiselevskiy[3], Yuri Legenkiy[2], Andrey Popandopulo[1]

Received: 20 Feb 2025 Published: 8 Jul 2025

Abstract

Background: Magnetic cell targeting holds significant promise for advancing cell therapy. This study reviewed recent experimental research on the use of magnetic particles for targeting mammalian cells in animal models, focusing on trends and therapeutic outcomes over the past five years.

Methods: A systematic search of PubMed, Cochrane Library, and eLibrary (2019–September 2024) was conducted using keywords: "magnetic cell targeting," "magnetic cell delivery," "magnetic cell localisation," and "magnetic cell guidance," excluding "drug." Inclusion criteria: original animal studies using mammalian cells labeled with magnetic nano- or microparticles and targeted via magnetic fields. Exclusion criteria included reviews, subcellular structures targeting, hyperthermia, tissue engineering, and in vitro-only studies.

Results: Of 10,908 studies, 39 met the criteria. Research focused on the nervous system (39%), cancer (10%), eye (10%), urinary tract (10%), heart (8%), and musculoskeletal diseases (8%). Targeted cells included mesenchymal stromal cells (59%), immune cells (15%), endothelial cells (13%), and others. Superparamagnetic iron oxide nanoparticles (37 studies) or microparticles (2 studies) were used, with sizes of 10–170 nm (95%) or 1–2.8 µm. Common coatings included poly-L-lysine, dextran, polydopamine, and silica. Labeling concentrations ranged from 20–100 µg Fe/ml (81%), with 4–24 hours incubation. Permanent magnets (95%, primarily neodymium) with 0.005–1.45 T induction were used. Magnetic targeting increased local cell concentration by 1.16–20 times in 19 studies and enhanced therapeutic effects in 85% of cases, though one study reported inferior results.

Conclusion: Magnetic cell targeting demonstrates significant potential for enhancing cell therapy efficacy, with improved local cell retention and therapeutic outcomes in diverse disease models. Further research is needed to optimize protocols and expand clinical applications.

Keywords: Cell therapy, Cell engineering, Magnetics, Magnetic iron oxide nanoparticles

Conflicts of Interest: *None declared*
Funding: *This work was supported by the Ministry of Health of the Russian Federation as part of a state assignment No. ZUNQ-2025-0002.*

This work has been published under CC BY-NC-SA 4.0 license.
Copyright© Iran University of Medical Sciences

Cite this article as: Turchin V, Ishchenko R, Bespalova S, Solopov M, Kiselevskiy M, Legenkiy Y, Popandopulo A. The Application of Magnetic Particles for Cell Targeting in Preclinical Animal Models: A Systematic Review. *Med J Islam Repub Iran.* 2025 (8 Jul);39:91. https://doi.org/10.47176/mjiri.39.91

Introduction

Cell therapy is a fundamental approach to regenerative medicine. Its ongoing development and potential are linked to the ability to treat diseases that have no effective therapeutic alternative within the conventional medical repertoire, particularly with regard to structural and functional regeneration. This applies, for example, to neuro-

Corresponding author: *Viktor Turchin, turchin.dn@mail.ru*

1. V.K. Gusak Institute of Emergency and Reconstructive Surgery of the Ministry of Health of the Russian Federation, Donetsk, Russia
2. Donetsk State University, Donetsk, Russia
3. N.N. Blokhin National Medical Research Center of Oncology of the Ministry of Health of the Russian Federation, Moscow, Russia

↑What is "already known" in this topic:
Labeling of cells with magnetic nano- or microparticles (predominantly iron oxide based) allows the localization of the cells into desired site. Potentially it can be used to increase effectiveness of cell therapy by increasing of local concentration of therapeutic grate cells in injury site.

→What this article adds:
This study summarizes the data on implementation of magnetic cell targeting using magnetic particles in animal models for the last 5 years. The study provides insights into the extent of local cell concentration enhancement and the therapeutic effects on animal disease models resulting from the application of magnetic cell targeting.

[Downloaded from mjiri.iums.ac.ir on 2026-10-14]

[DOI: 10.47176/mjiri.39.91]

degenerative diseases (1, 2), type 1 diabetes (3), traumatic nervous system injuries (4), degenerative processes in cartilage tissue (5), and others. In the context of the ongoing shortage of donor organs, cell therapy may serve as an alternative to organ transplantation (6, 7). The therapeutic effect of cells introduced into the body is primarily mediated by the replacement of damaged or aging cells or by paracrine mechanisms, such as the secretion of growth factors, cytokines, cytoprotective factors, and other biologically active substances. Therefore, the therapeutic efficacy of cell therapy is, among other factors, closely dependent on the concentration of cells at the site of tissue damage (8, 9). The concentration and retention of injected cells at the target site can be hindered by the complex anatomical and physiological characteristics of organs and tissues (e.g., the blood-brain barrier (10), ocular structures (11, 12), vestibular or auditory apparatus (13), functioning heart (14, 15), joints (16)), as well as their pathological conditions (e.g., ischemia (17, 18), microcirculatory disturbances and inflammatory microenvironment (19, 20)), which alter the local cytokine and receptor landscape, thereby preventing effective cell homing. According to Devine S.M. et al. (21), the implantation efficiency of multipotent mesenchymal stromal cells (MMSCs) after systemic administration is only 0.1-2.7%.

Magnetic targeting is a promising strategy for enhancing the efficiency of cell delivery and retention following injection into the body (22–25). This method involves two main steps: labeling cells with magnetic nanoparticles or microparticles and capturing them at the target site using a magnetic field (a "magnetic trap"). Additionally, magnetic fields can be used to control the spatial organization of cells (26), as well as their adhesion and aggregation density – features that are particularly important for applications such as cartilage regeneration (16, 27). The primary objective of magnetic cell labeling is to achieve an optimal balance between magnetic responsiveness and the preservation of cell viability and functionality required for therapeutic efficacy. A key aspect of magnetic trap design is to generate a sufficient magnetic field strength gradient at the target site. Notably, magnetic particles (MPs) also provide magnetic contrast, enabling in-vivo tracking of the particles and associated cells using magnetic resonance imaging (MRI) after their introduction into the body (12, 28, 29).

This paper aims to review experimental studies from the past 5 years focusing on the application of magnetic particles for cell targeting in animal models. The objective is to identify current trends, methodologies, and experimental models employed, as well as to assess therapeutic outcomes. Over the past 5 years, only one systematic review addressing a similar topic has been published, covering studies conducted from January 2000 to July 2018 (30). However, that review was limited to data involving stem cells and superparamagnetic iron oxide nanoparticles (SPIONs) as labeling agents. Therefore, this study serves to update and expand the existing data in this area of research.

Methods

Search strategy

The present systematic review was conducted in accordance with the PRISMA 2020 guidelines for systematic reviews (31). Studies were identified through searches of the PubMed, Cochrane Library, and eLibrary bibliographic databases for the period from 2019 to September 2024. For PubMed and the Cochrane Library, the search terms included “magnetic cell targeting”, “magnetic cell delivery”, “magnetic cell localisation”, and “magnetic cell guidance”. The term "drug" was excluded from the searches. The exclusion was applied to eliminate the substantial number of publications related to magnetic drug delivery, which fall outside the scope of this review. In eLibrary, in addition to the aforementioned keywords, the search also included the Russian-language terms “магнитное нацеливание клеток” (magnetic cell targeting) and “магнитная доставка клеток” (magnetic cell delivery). The search strategies and the primary results from each database are summarized in Table 1. Duplicate records identified across the different databases were removed (Figure 1).

Study PICO

Population: Animals (mice, rats, rabbits, etc.) used in experimental disease models.

Intervention: Application of magnetic nano- or microparticles (primarily iron oxide) for labeling mammalian cells (e.g., mesenchymal stromal cells, immune cells, endothelial cells, etc.).

Comparator: Absence of magnetic field exposure (control groups).

Outcome: Increased local cell concentration in the target area; enhanced therapeutic effects in various diseases (e.g., reduced inflammation, tissue regeneration, improved organ function); evaluation of the safety and efficacy of magnetic cell targeting.

Table 1. Search queries and search results

Bibliographic database	Query	Date of search	Result
PubMed	(((magnetic cell targeting) OR (magnetic cell delivery) OR (magnetic cell localization) OR (magnetic cell guidance))) NOT (drug) AND (2019:2024[pdat])	05.10.2024	8207
Cochrane Library	magnetic cell targeting in All Text OR magnetic cell delivery in All Text OR magnetic cell localization in All Text OR magnetic cell guidance in All Text NOT drug in All Text - publication date Between Jan 2019 and Sep 2024	12.10.2024	1297
eLibrary	((magnetic cell targeting) or (magnetic cell delivery) or (magnetic cell localization) or (magnetic cell guidance) or (магнитное нацеливание клеток) or (магнитная доставка клеток)) &! drug Filters: scientific journal articles; 2019-2024.	12.10.2024	1404

[Downloaded from mjiri.iums.ac.ir on 2026-10-14]

[DOI: 10.47176/mjiri.39.91]

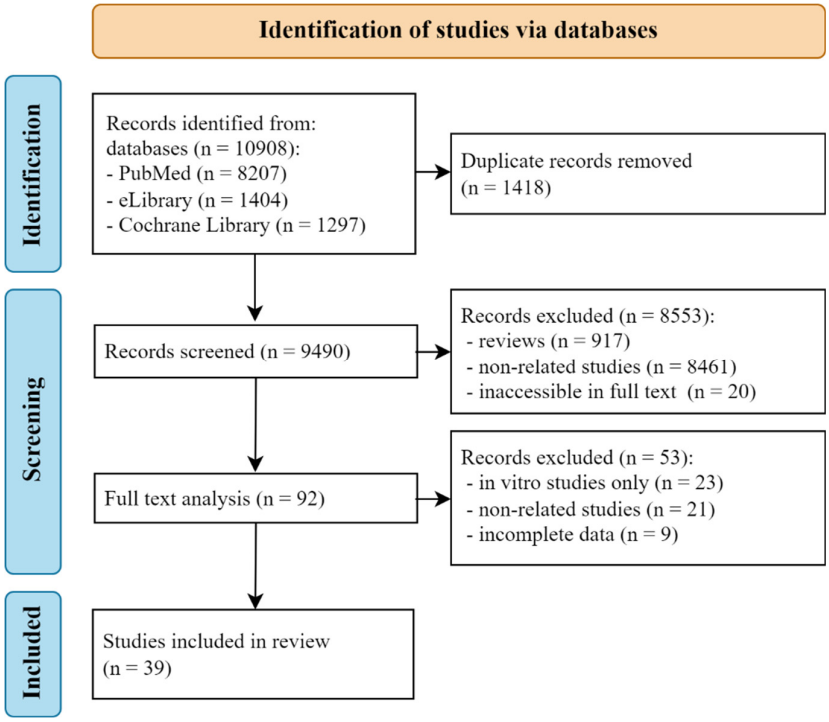

Figure 1. PRISMA flow diagram for literature search strategy

Screening and selection of the studies

Screening of search results according to the inclusion and exclusion criteria was independently conducted by two researchers (Viktor Turchin and Maxim Solopov). Discrepancies were resolved by a third researcher (Andrey Popandopulo or Mikhail Kiselevsky).

Inclusion and exclusion criteria

During the screening stage, papers were selected based on the following inclusion criteria: 1) original research involving laboratory animals; 2) use of human or mammalian cells; 3) application of magnetic nano- or microparticles for cell labeling; 4) employment of magnetic fields to target and retain cells within a specific region of interest in an animal model. Only full-text articles available in the specified bibliographic databases, on publishers' websites, publicly accessible online platforms, or obtained directly from the authors were included in the study.

The following types of studies were excluded: 1) review articles; 2) studies focusing on magnetic delivery of subcellular components or prokaryotic cells; 3) magnetic separation of cells or organoids; 4) hyperthermia therapy; 5) magnetic tissue engineering; 6) magnetic microcarrier applications; 7) MRI contrast enhancement or magnetic stimulation of cells without magnetic targeting; 8) magnetic targeting of cells in in vitro studies only.

Data extraction

Data extraction performed by Viktor Turchin, Maxim Solopov, and Yuri Legenkiy. During the article's processing, data were collected on the study design, cell cultures used, and the key characteristics of the magnetic particles, including hydrodynamic size, stabilizing shell, and surface charge. Information on the magnetic labeling conditions was also recorded, such as the concentration of magnetic particles in the labeling solution and the labeling duration. For the in vitro stage of the study (where applicable), data were gathered on the type of experiment, the characteristics of the magnetic trap, and the primary results. For the in vivo stage, information was collected on the animal models, route of administration, cell dose, magnetic trap specifications, magnetic field exposure duration, observation period, and main outcomes. The evaluation of in vivo studies emphasized the effects of magnetic targeting. This was achieved by comparing groups differing only in the use of the magnetic trap, while all other conditions were kept constant.

Quality assessment

To assess the methodological quality of individual animal studies, the SYRCLE's (SYstematic Review Centre for Laboratory animal Experimentation) risk of bias tool for animal studies was applied based on several criteria (32). Each criterion was judged as "Low," "High," or "Unclear" risk of bias based on signaling questions. Two reviewers (V.T. and M.S.) independently assessed biases, resolving discrepancies through consensus.

Selection bias:

- Sequence generation: Assess whether the allocation sequence was randomly generated.
- Baseline characteristics: Evaluate whether the groups were similar at baseline or if adjustments were made for

[Downloaded from mjiri.iums.ac.ir on 2026-10-14]

[DOI: 10.47176/mjiri.39.91]

potential confounders.

• Allocation concealment: Determine whether allocation was concealed to prevent anticipation of group assignments.

Performance bias:

• Random housing: Verify whether animals were randomly housed to minimize environmental bias.

• Blinding of caregivers/investigators: Assess whether personnel administering interventions were blinded to prevent differential treatment.

Detection bias:

• Random outcome assessment: Confirm whether animals were randomly selected for outcome measurement to avoid circadian rhythm effects or subjective selection.

• Blinding of outcome assessors: Ensure that outcome assessors were blinded to group assignments and that assessment methods were consistent across groups.

Reporting bias:

• Selective outcome reporting: Determine whether all pre-specified outcomes were reported by comparing the methods section to the results or by referencing a study protocol.

Other bias:

• Unit-of-analysis errors: Check whether the correct experimental unit was used in the analysis.

• Contamination/funding influence: Assess whether there was unintended treatment pooling or potential bias related to funding sources.

• Other potential influences.

Results

A total of 39 articles were selected for the study. A summary of the animal models and parameters of the in vivo phase of the studies is provided in Table 2 and Appendix Table A1. Of these, 21 articles (54%) included an in vitro phase, with the corresponding data presented in Appendix Table A2.

MMSCs were the most commonly used target for magnetic labeling, reported in 23 studies (59%). Immune system cells were utilized in 6 studies (15%), endothelial cells and their progenitors were studied in 5 studies (13%), while other cell types were investigated in another five studies (13%).

The studies utilized SPIONs with primary dimensions of 10–170 nm (37 studies, 95%) or microparticles of iron oxide (MPIOs) with sizes of 1 and 2.8 μm (2 studies, 5%). Various stabilizing shells were used for cell labeling, with 18 different types reported. The zeta-potential of the particles ranged from −52 to +64.9 mV, with 77% of the particles exhibiting a negative charge. Optimal labeling concentrations were reported to be within the range of 20-100 μg Fe/mL in 81% of cases, while labeling durations ranged from 4 to 24 hours.

In vitro stage of magnetic targeting studies

In 21 studies (54%), in vitro magnetic targeting experiments were conducted prior to the in vivo phase (Appendix Table A2). These experiments aimed to evaluate the efficiency of magnetic labeling and the magnetic susceptibility of cells, optimize magnetic trap parameters, and address other tasks essential for designing the in vivo stage of the study.

Among the analyzed studies, several groups of commonly used methods and approaches can be distinguished. The most technically simple approach involved passive trapping of magnetically labeled cells (10 studies), which makes it possible to assess the ability of cells to accumulate in the zone of the greatest magnetic field gradient, usually in a culture dish.

The assessment of cell migration activity (vertical migration) in a magnetic field was conducted in 7 studies using a Transwell chamber, which models the conditions of biological barriers and tissue infiltration. For MMSCs, endothelial progenitor cells (EPCs), endothelial cells, and neutrophils, an increase in vertical migration under the influence of a magnetic field by 1.5–3.3 times was demonstrated (13, 15, 29, 33, 34). For T-lymphocytes, the increase was 10–11.5% (35, 36). Horizontal migration was also assessed in four studies for MMSCs and dendritic cells (DCs).

Cell capture under flow conditions was studied in nine papers, enabling the evaluation of magnetic capture efficiency within vascular-like environments. For this purpose, channel slides, microfluidic chips, and vascular phantoms connected to circulation systems were employed. Alternatively, orbital shakers and rotary devices were used to simulate flow conditions. Flow rates ranged from 0.1 to 1 mL/min in most studies, with one study reporting a flow rate of 14.6 mL/min (18). Magnetic capture efficiency was shown to depend on flow rate, shear stress, cell labeling method, and magnetic field induction, with reported values ranging from 25% to >95% (18, 22, 37).

Other methods were also used to evaluate magnetic targeting in vitro, including vertical and horizontal migration of MMSCs in hydrogel (25, 37), within porous scaffolds and in a hanging drop against gravitational force (37), and migration through a microfluidic channel with obstacles was also assessed (38). For DCs, the ability to enhance adhesion to a monolayer of Caco-2 cells under the influence of a magnetic field was evaluated (23). To assess biocompatibility and functional activity, magnetically labeled endothelial cells were captured in suspension using a 3D-printed implantable magnetic device (“epicardial patch”), followed by cell incubation on the device (15).

In vivo stage of magnetic targeting studies

Distribution of studies by cell type and animal disease models

Among the in vivo studies, the largest proportion focused on models of nervous system disorders (14 studies, 39%), primarily ischemic (6 studies) and neurodegenerative (5 studies) diseases. A notable number of studies were also conducted on models of urinary system diseases (4 studies), eye diseases (4 studies), oncological diseases (4 studies), ischemic heart diseases (3 studies), musculoskeletal disorders (2 studies), and other animal models (8 studies) (Figure 2).

As shown in Figure 2, of the 39 studies conducted on animal models of disease, 23 (59%) utilized MMSCs.

[Downloaded from mjiri.iums.ac.ir on 2026-10-14]

[DOI: 10.47176/mjiri.39.91]

Table 2. Experimental parameters and outcomes of magnetic cell targeting in in vivo models

Experimental design			Magnetic trap		Effects of magnetic targeting versus control	Ref.
Animal model	Cells, magnetic tag	Route of administration, cellular dose	Type, induction	Time of action		
Nervous system disease models						
Rats, sciatic nerve injury	MMSCs, SPION-Cit	IV, 6-7x10^6/300 µl NaCl 0,9%	NdFeB, 0,16 T	24 hours	After 6 days ↑ myelination and nerve conduction.	(46)
Rats, neonatal hypoxia of the brain	MMSCs, SPION-PLL	ICV, 10^5/5 µl	NdFeB, 0,39 T	2 hours	After 4 weeks ↑ diffusion indices and ↓ apoptosis.	(48)
Rats, neonatal cerebral arterial thrombosis	Erythrocytes, SPION-biotin-streptavidin-SiO_2	IV, equivalent to 6 mg Fe/kg	NdFeB, 0,5 pN	10 hours	After 30 min - hypoperfusion, after 6 h - neurodegeneration, after 7 h - cerebral infarction.	(47)
Rats, cerebral hypoxia	MMSCs, SPION-PLL	ICV, 10^5/5 µl	NdFeB, 0,118 T	2 hours	After 4 weeks ↓ tissue kurtosis, swelling, microglia infiltration and apoptosis levels.	(17)
Rats, intracerebral hemorrhage	Spherical neuronal masses, FION	IV, 4x10^6/500 µl PBS	Two NdFeB, 0,32 T	3 days	After 3 days ↓ swelling and inflammation. After 42 days ↓ brain atrophy.	(19)
Mice, cerebral infarction	MMSCs, SPION- polydopamine	IV, 5x10^5 в PBS (24 h after surgery)	Permanent magnet	5 days	↓ infarct area and microglia activity, ↑ expression of neuronal factors.	(49)
Rats, carotid artery trauma	MMSCs, nanocapsules-SPION-PLGA-PEG	Intraarterially, 5x10^6/20 µl PBS	Two permanent magnets 0,3 T	5 minutes	↑ cell retention in the area of vascular injury with effects lasting 24 hours.	(25)
Albino rats, facial nerve palsy	MMSCs, SPION-PLL	IV, 10^6/0,2 ml culture medium	NdFeB, 0,57 T	24 hours	Facial nerve regeneration is below control values.	(28)
Mice, Alzheimer's disease	MMSCs, SPION- polydopamine	IV, 2x10^5/100 µl	NdFeB	12 hours	After 10 days, ↑ number of MMSCs in hippocampus; ↑ memory.	(50)
Rats, Alzheimer's disease	MMSCs, SPION-dextran	ICV, IV, 10^6/animal	Halbach array, 0,2 T	2 hours	After 8 weeks ↑ memory and cognitive function. After 10 weeks ↑ expression of ChAT and AChE and ↓ apoptosis.	(39)
Mice, Alzheimer's disease	MMSCs, SPION	ICV, 10^5/7 µl	Permanent magnet	3 days	After 7 days ↓ amyloid β levels. ↑ cognitive functions with repeated injections after 3 weeks.	(22)
Rats, Parkinson's disease	MMSCs, SPION-PLL	Locally, 3x10^5/9 µl NaCl 0,9%	NdFeB, 0,32 T	1 week	↑ motor function after 3 and 6 weeks.	(51)
Rats, Parkinson's disease	MMSCs, SPION-alginate	Intranasal drip	Halbach array, 0,2 T	8 weeks	After 4 weeks ↑ motor functions, after 8 weeks restoration of the dopaminergic system.	(40)
Athymic mice	MMSCs, SPION-PLL	Locally, 10^6/10 µl PBS	Permanent magnet, 0,02 T	2 days	MMSCs were detected in the brain only in the magnetic field group.	(38)
Models of urinary system diseases						
Rabbits, anterior bladder wall resection	MMSCs, SPION (ferucarbotran)	Locally, 10^6/animal	NdFeB, 1 T	10 minutes	After 14 days ↑ repair, vascularization and volume of myofibrotic tissue.	(45)
Rats, stress urinary incontinence	Myoblasts, SPION-PVP-PLL	Locally, 1,5x10^6/200 µl PBS	NdFeB, 0,19 T	20 minutes	After 14 days ↑ urethral sphincter thickness and normalization of leak point pressure.	(52)
Mice, diabetic nephropathy	MMSCs, SPION- polydopamine	IV, 5x10^5/200 µl PBS	Permanent magnet, 1,2 T	20 minutes	After 28 days ↑ renal function, ↓ inflammation and nephropathy.	(53)
Rats, renal ischemia-reperfusion injury	EPCs, SPION-PEG-anti-CD-133	IV, 2x10^6/200 µl PBS	Permanent magnet	30 minutes	After 3 days ↑ renal function, ↓ apoptosis and ↑ proliferation of renal parenchyma.	(33)

[Downloaded from mjiri.iums.ac.ir on 2026-10-14]

[DOI: 10.47176/mjiri.39.91]

Table 2. Experimental parameters and outcomes of magnetic cell targeting in in vivo models

Experimental design			Magnetic trap		Effects of magnetic targeting versus control	Ref.
Animal model	Cells, magnetic tag	Route of administration, cellular dose	Type, induction	Time of action		
Models of eye diseases						
Mice, glaucoma	TMCs, SPION- PLGA	Locally, $75x10^3$/3 µl	Ring magnet, 0,06 T	15-45 minutes	Temporary ↓ intraocular pressure for 10 days.	(12)
Mice, glaucoma	MMSCs, TMCs, SPI-ON-amine	Locally, $1,5x10^3$/1,5 µl	NdFeB, 0,25 T	No data	↓ intraocular pressure at 9 and 4 months by the use of MMSCs and TMCs respectively.	(11)
Rabbits, corneal endothelial dysfunction	Corneal endothelial cells, SPION-SiO_2	Locally, 2-$6x10^5$/100-250 µl Hanks' solution	NdFeB	3 hours	After 7 days ↓ corneal edema. After 14 days ↑ corneal transparency.	(42)
Chinchilla rabbits	MMSCs, MPIO-Pluronic L-123	Locally, 10^4/50 µl culture medium	Permanent magnet, 5 mT	15 days	Retention of hypoxic MMSCs under the retina for 9 days.	(43)
Models of ischemic heart diseases						
Mice, cardiac ischemia-reperfusion injury	MMSCs, SPION-SiO_2-IGF	Locally, 10^5/20 µl culture medium	Permanent magnet	7 days	↑ contractile function, ↓ cardiomegaly and fibrosis.	(18)
Rats, myocardial infarction	Rat endothelial cells, SPION (FluidMAG D)	Locally as part of the implant	Magnetic epicardial implant	28 days	After 14 days ↑ angiogenesis and perfusion. After 28 days ↑ contractile function, ↓ infarct area and fibrosis.	(15)
Rats, myocardial infarction	EPCs, SPION-SiO_2	IV, 10^6/100 µl PBS	Permanent magnet, 0,39 T	1 hour	After 4 weeks ↑ contractile function and angiogenesis, ↓ myocardial infarct area, fibrosis and apoptosis.	(14)
Cancer disease models						
Mice, lymphoma	CTLs, SPION-APS	IV, $8x10^6$/100 µl PBS	NdFeB, 1,45 T	90 minutes	After 14 days, ↓ tumor infiltration and ↑ CTLs activity in lymph nodes.	(35)
Mice, lymphoma and breast cancer	CTLs and TILs, SPION-PEG-anti-PD-1	IV, 0,5-$1x10^7$/animal	NdFeB	12 hours	↑ tumor infiltration of CTLs and TILs by ~3-fold. Complete tumor suppression and 100% survival at 35 days in groups with magnet.	(24)
Mice, sarcoma	DCs, SPION-antigens to Sa-37	Locally, 10^6/animal	NdFeB, 20 pN	1 hour	After 28 days ↓ tumor growth and changes in the expression of cytokines and angiogenesis factors.	(44)
Mice, brain glioma	Neutrophils, SPION-gelatin	IV, $3*10^6$/animal	RMF device	1 hour	↑ average survival time.	(29)
Models of musculoskeletal diseases						
Mice, myositis	MMSCs, anionic SPION liposomes	Locally, $5x10^5$/ animal	Permanent magnet	3 hours	After 5 days ↓ levels of inflammatory cytokines.	(20)
Rabbits, osteoarthritis	Chondrocytes, SPION-gelatin	Locally	Permanent magnet	8 weeks	After 8 weeks ↑ the level of proteoglycans in the joint.	(16)
Other animal models						
Mice, silicosis of the lungs	MMSCs, SPION-Cit	IV, $3x10^5$/50 µl NaCl 0,9%	Two NdFeB	48 hours	↓ static lung elasticity, resistive pressure, granuloma area and IL-1β levels.	(34)
Mice, ototoxicity model	MMSCs, SPION-PLGA	IV	NdFeB	24 hours	↑ of local concentration of MMSCs.	(13)
Rat, full-thickness skin burns	MMSCs, SPION-SDS	IV, 10^6/1 ml PBS	NdFeB, 1,2 T	30 minutes	After 7 days ↑ angiogenesis, ↓ inflammation.	(54)

[Downloaded from mjiri.iums.ac.ir on 2026-10-14]

[DOI: 10.47176/mjiri.39.91]

Table 2. Experimental parameters and outcomes of magnetic cell targeting in in vivo models

Experimental design			Magnetic trap		Effects of magnetic targeting versus control	Ref.
Animal model	Cells, magnetic tag	Route of administration, cellular dose	Type, induction	Time of action		
Other animal models						
Athymic mice	T-cells, SPION-APS	IV, 10^7/100 µl	NdFeB, 1,45 T	30-90 minutes	↑ homing to the lymph nodes.	(36)
Rats, type I diabetes mellitus	MMSCs, SPION- polydopamine	IV, 10^6/1 ml PBS	NdFeB, 1,2 T	30 minutes	After 3 weeks ↓ β-cell apoptosis.	(55)
Healthy mice	Erythrocytes, SPION-DMSA	IV, 315x10^6 in 300 µl	Electromagnet, 0,8 T	30 minutes	Intravascular formation of erythrocyte aggregates in a magnetic field stable for 6 h.	(41)
Healthy rats	MMSCs, MPIO-SiO_2 (SiMAG)	Locally, 10^6/100 µl	NdFeB, 0,3 T	20 minutes	↑ of local concentration of MMSCs.	(37)
Healthy mice	Macrophages, cationic SPION liposomes	Locally, 10^6/animal	Permanent magnet	1 hour	↑ cell retention in the rectum for 24 h.	(23)

Abbreviations: AChE – acetylcholinesterase; APS – 3-aminopropyltriethoxysilane; ChAT – choline acetyltransferase; Cit – citrate; COX-2 – cyclooxygenase-2; CTLs – cytotoxic T lymphocytes; DMSA – dimercaptosuccinic acid; EPCs – endothelial progenitor cells; ESCs – embryonic stem cells; FION – ferrimagnetic iron oxide nanocubes; ICV – intracerebroventricular; IL – interleukin; IV – intravenous; MAP2 – microtubule-associated protein 2; MPIO – microparticles of iron oxide; MRI – magnetic resonance imaging; MMSCs – multipotent mesenchymal stromal cells; NdFeB – neodymium-iron-boron; NeuN – neuronal nuclear antigen; PBS – phosphate-buffered saline; PEG – polyethylene glycol; PLGA – poly(lactic-co-glycolic acid); PLL – poly-L-lysine; pN – piconewton; PVP – polyvinylpyrrolidone; RMF – rotating magnetic field; SPION – superparamagnetic iron oxide nanoparticles; TILs – tumor-infiltrating lymphocytes; T – Tesla (the unit of magnetic flux density); TMCs – trabecular meshwork cells.

[Downloaded from mjiri.iums.ac.ir on 2026-10-14]

[DOI: 10.47176/mjiri.39.91]

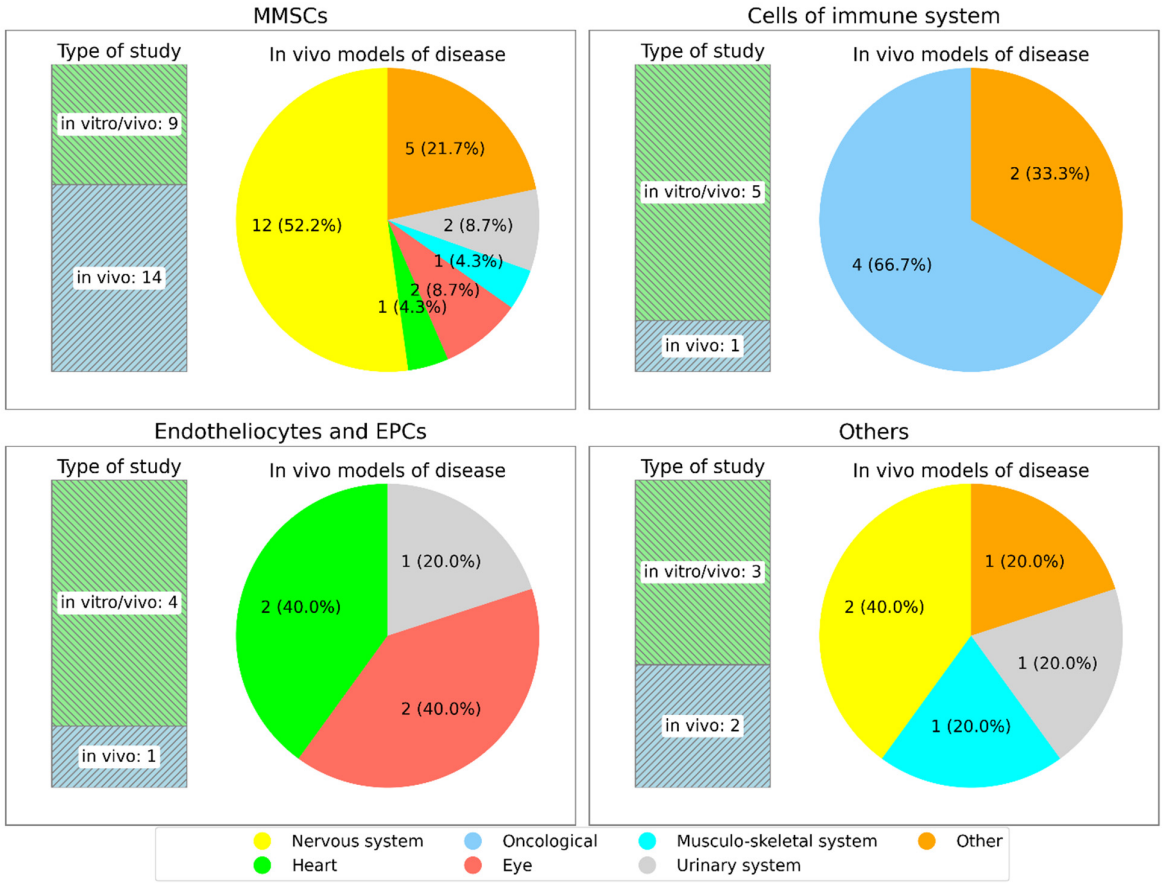

Figure 2. Distribution of studies by category of magnetically labeled cells, in vivo disease models, and study types. Abbreviations: EPCs – endothelial progenitor cells; MMSCs – multipotent mesenchymal stromal cells.

[Downloaded from mjiri.iums.ac.ir on 2026-10-14]

[DOI: 10.47176/mjiri.39.91]

These studies predominantly focused on nervous system disorders (12 articles), including neurodegenerative diseases, ischemic brain injury, and peripheral nerve damage. MMSCs were also used in models of eye diseases (glaucoma), musculoskeletal conditions (muscle inflammation), urinary system disorders (diabetic nephropathy, bladder resection), and other diseases, such as pulmonary silicosis, diabetes mellitus, skin burns, and hearing loss.

Immune system cells, including T cells, DCs, and neutrophils, were primarily employed in cancer models (4 articles). Macrophages were used in models of rectal inflammation, and T cells were studied in the lymph nodes of healthy animals.

Endothelial cells and EPCs were investigated in models of myocardial infarction, glaucoma, corneal injury, and renal ischemia-reperfusion injury.

Other cell types were used in specific models, including neuronal progenitor cells (NPCs) for intracerebral hemorrhage, myoblasts for stress urinary incontinence, chondrocytes for osteoarthritis, and erythrocytes for modeling cerebral ischemia via intravascular aggregation under a magnetic field.

Magnetic traps

In 95% of the analyzed in vivo studies (37 publications), permanent magnets, predominantly neodymium magnets (24 studies) were used as magnetic traps. These magnets varied in shape, size, and magnetic induction, tailored to the specific animal models. For example, a Halbach array used in studies on models of Alzheimer's disease (39) and Parkinson's disease (40), and a small ring magnet employed in a mouse model of glaucoma (12). Two studies utilized alternative magnetic traps: an electromagnet with a maximum induction of 0.8 T (41) and a rotating magnetic field device (29).

Magnetic cell capture/retention efficiency

The main purpose of magnetic targeting of cells in vivo is to increase their local concentration in the target area after administration, which is achieved both by capturing circulating cells (usually after systemic administration) and by retaining cells (mainly after local administration). The results of magnetic targeting in the reviewed studies were determined in several ways, of which the most commonly used method was the detection of the fluorescent label (12, 42, 43), carried either by the cells them-

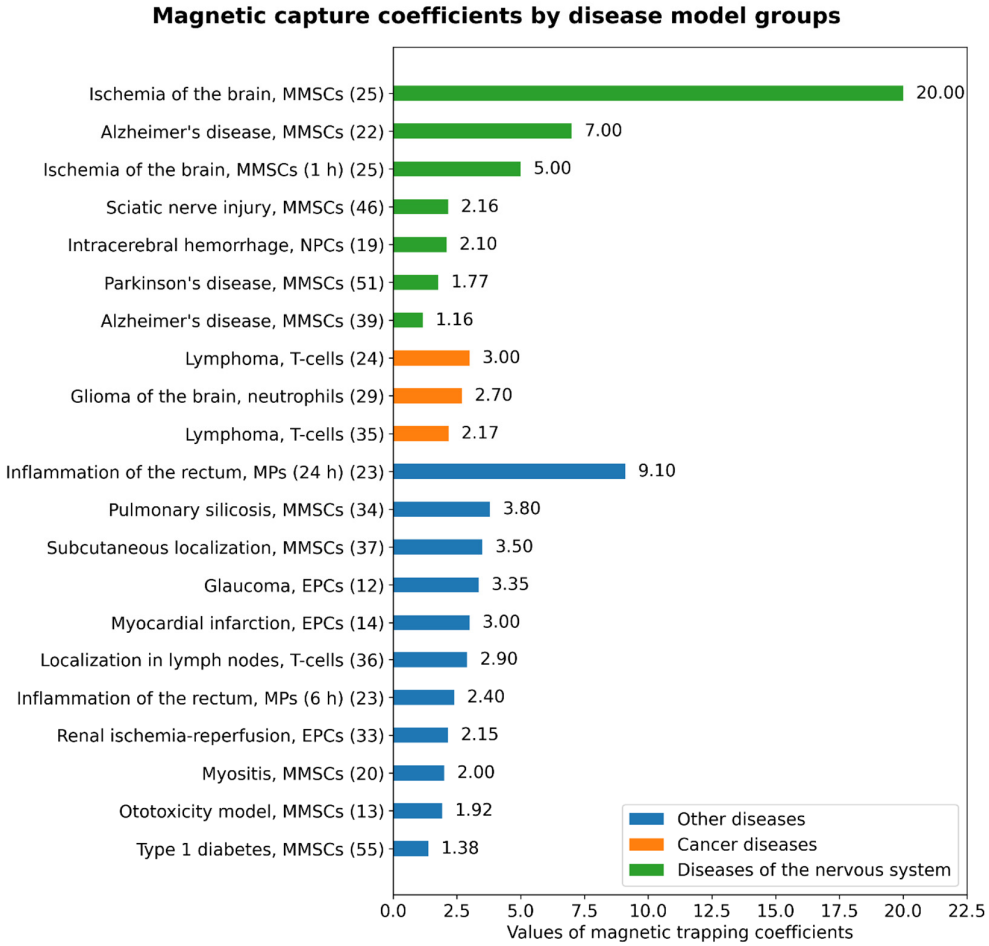

Figure 3. Magnetic capture coefficients of different cell types in animal models of disease. Abbreviations: EPCs – endothelial progenitor cells; MMSCs – multipotent mesenchymal stromal cells; MPs – macrophages; NPCs – neuronal progenitor cells.

[Downloaded from mjiri.iums.ac.ir on 2026-10-14]

[DOI: 10.47176/mjiri.39.91]

selves or by the MPs used for labelling. Histochemical methods of detection (29, 35, 40, 44–46) as well as MRI, typically in T2 mode (12, 28, 29), and other methods were also used.

In the 19 studies reviewed, quantitative data on the results of magnetic targeting were obtained. These data are presented in Figure 3 as magnetic capture coefficients, which were calculated by comparing the local cellular concentration in experimental groups that differed only in the use of the magnetic field. As demonstrated by the data, magnetic targeting leads to a significant increase in local cell concentration after administration, ranging from 1.16 up to 20 times.

Unexpectedly, we revealed no significant correlations (data not shown) between magnetic cell capture/retention efficiency and the following parameters: magnetic field strength, magnetic field exposure duration, magnetic particle size, surface charge and shell composition, cell type, incubation time with magnetic particles, labeling concentration, and intracellular iron content. This observation is likely attributable to the substantial heterogeneity among the reviewed studies, encompassing variations in experimental design, cell types, magnetic nanoparticle formulations, and in vivo cell tracking methodologies.

Therapeutic effects

Excluding studies involving healthy animals (23, 37, 38) and the use of magnetic erythrocytes to model vascular thrombosis (41, 47), most of the analyzed studies found that the effect of magnetic targeting was associated with a positive therapeutic outcome, which corresponded to the disease model and the applied cell type. However, one study reported that the outcome of magnetic targeting of MMSCs for the treatment of facial nerve injury was lower than that of the control (28). The authors attributed this to the toxic effects (oxidative stress) caused by the SPION labeling of the cells.

The main therapeutic effects observed in the analyzed studies, categorized by disease model, are summarized below. The data presented result from the comparison between experimental groups that differed only in the application of the magnetic field, thus reflecting the effect of magnetic cell targeting. Additional details on the experimental design of the in vivo studies and the conditions for cell labeling are available in Table 2 and Appendix Table A1.

Models of ischemic brain injuries

In a model of hypoxic-ischemic brain injury in newborn rats (48), 4 weeks after the administration and magnetic capture of MMSCs in the injury area, improvements were observed in local blood flow recovery, specifically a 65% increase in the diffusion coefficient and a 33% increase in the diffusion fraction, along with a 60-fold reduction in neuronal apoptosis. On a similar model in adult rats, in a study by the same research group (17), a reduction in neuronal apoptosis, a decrease in average brain edema, a reduction in microglial infiltration, and, according to MRI data, a two-fold decrease in mean kurtosis in the injury zone were also observed, indicating recovery of tissue microstructure.

The application of magnetic targeting of MMSCs in a mouse model of cerebral infarction (49) after 5 days resulted in 41% reduction of the infarct area, shift of local microglia balance towards the M2 phenotype, as well as increased expression of neuronal proteins MAP2 and NeuN by 26% and 30%, respectively, which indicates activation of neuroprotective mechanisms and neuroregeneration in the infarct area.

In a rat model of intracerebral hemorrhage (19) magnetic targeting of spherical neuronal masses (neuronal progenitors) derived from embryonic stem cells (ESCs) led to a 2.1-fold concentration of cells in the injury zone 3 days after intravenous administration. This was accompanied by a reduction in brain edema, a 2-fold decrease in IL-1β levels, a 17% decrease in pERK expression, and a 2.8-fold decrease in COX-2 levels. The level of brain atrophy was 36% lower than that of the control group 42 days after cell administration.

In summary, the presented data suggest that magnetic targeting of MMSCs and neuronal progenitors positively impacts disease outcomes in various models of ischemic brain injury in laboratory animals by activating neuroprotective mechanisms, promoting regenerative processes, and modulating inflammatory responses.

Models of neurodegenerative diseases

In an experiment conducted on transgenic mice with an Alzheimer's disease model (APP/PS1) (50), magnetic targeting of MMSCs facilitated their accumulation in the hippocampus within 10 days after administration. This was accompanied by an improvement in cognitive functions in the animals, particularly spatial memory, as evidenced by a 43% enhancement in water maze test performance. Additionally, an increase in synaptophysin and BDNF (brain-derived neurotrophic factor) expression was observed in neurons, indicating the activation of neuroprotective and neuroregenerative mechanisms.

In another transgenic mouse model of Alzheimer's disease (5xFAD) (22), magnetic targeting of MMSCs over three days following intracerebroventricular administration resulted in a 7-fold increase in the number of cells within the damaged brain region. By day 7, a 44% reduction in β-amyloid levels was observed. After three repeated cell administrations, cognitive functions improved by 24–60% three weeks after the final injection.

In a rat model of Alzheimer's disease (39), magnetic targeting of MMSCs following intravenous administration using a Halbach array for 2 hours resulted in a 16% increase in cell accumulation in the hippocampus 8 weeks post-injection. This approach improved memory and cognitive functions by 24–58%, as assessed by the passive avoidance response and Morris water maze test. Ten weeks after cell administration, there was a 28% and 20% increase in the expression levels of choline acetyltransferase (ChAT) and acetylcholinesterase (AChE), respectively, along with a 59% reduction in neuronal apoptosis.

In a rat model of Parkinson's disease (51) 7 days of magnetic targeting of MMSCs following their local administration to the affected brain region resulted in a 77% increase in the local cell concentration. 3 and 6 weeks

[Downloaded from mjiri.iums.ac.ir on 2026-10-14]

[DOI: 10.47176/mjiri.39.91]

after cell administration, improvements in the apomorphine-induced rotation test were observed at 15% and 22% respectively, indicating enhanced motor function in the experimental animals.

In another study on a rat model of Parkinson's disease (40), intranasal drip administration of MMSCs was combined with a Halbach array as a magnetic trap over 8 weeks. By week 4, motor function improvements were observed with an 85% enhancement in the rotarod test and a 53% improvement in the open field test. By week 8, histological analysis revealed a 63% increase in the number of dopaminergic neurons in the substantia nigra (the affected region) along with elevated expression levels of the proteins Nurr1, DAT, and Pitx3 by 32%, 11%, and 42% respectively, indicating restoration of the dopaminergic system.

The results demonstrate that magnetic targeting of MMSCs enhances cell concentration in affected brain regions and positively influences cognitive and motor functions in models of Alzheimer's and Parkinson's diseases. Increased expression of neurotrophic factors, reduction in β-amyloid levels, and restoration of the dopaminergic system indicate the ability of MSCs to activate neuroprotective and neuroregenerative processes in models of neurodegenerative diseases. These effects can be significantly amplified through magnetic targeting.

Models of nerve injury

In a rat model of traumatic sciatic nerve injury (46), magnetic targeting resulted in a 2.16-fold increase in the local concentration of MMSCs. 6 days post-injury, the damaged nerve showed a 3.8-fold increase in the number of myelinated axons, a 1.8-fold restoration of myelin basic protein levels (as determined by immunohistochemistry and Western blot), and a 2.12-fold reduction in distal latency. These findings indicate that the application of MSCs, particularly in combination with magnetic targeting, significantly enhances the structural and functional recovery of nerves.

In contrast, in a rat model of facial nerve injury (28) magnetic labeling and targeting of MMSCs resulted in poorer nerve function recovery compared to unlabeled MMSCs. A possible explanation for this is the toxic coating of SPIONs (poly-L-lysine), oxidative stress, and suboptimal labeling protocols.

Models of diseases of the urinary system

Short-term (within 10 minutes) magnetic targeting of MMSCs in a rabbit model of anterior bladder wall resection (45) resulted in a 2-fold increase in the area of tissue repair 14 days after cell administration. Additionally, there was a 2.3-fold increase in vascularization and the volume of myofibrous tissue, indicating active repair of the damaged tissue.

In a rat model of stress urinary incontinence (52), injection of MMSCs into the urethral sphincter area, followed by fixation of cells using a magnetic field for 20 minutes, increased cell retention in the target area. Fourteen days after injection, thickening of the urethral sphincter was observed. In all groups treated with MMSCs, the leak point pressure was comparable to that of the sham-operated group.

In a mouse model of diabetic nephropathy (53) 4 weeks after intravenous administration of MMSCs, the magnetic targeting group demonstrated increased cell concentration in the kidneys. This was accompanied by a 17% and 34% reduction in serum urea nitrogen and creatinine levels, respectively, as well as a 29% and 24% decrease in urinary creatinine and albumin levels. Additionally, kidney expression levels of IL-2 (by 34%), IL-6 (by 23%), IFN-γ (by 21%), TNF-α (by 40%), and plasma TGF-β (by 11%) were reduced. Across all groups receiving MMSCs, regardless of magnetic targeting, there was a notable decrease in macrophage infiltration, renal fibrosis, and inflammatory cytokine expression, a ~2-fold reduction in water consumption, a 20% increase in overall body weight, a 13% reduction in kidney weight, and a 25% reduction in the kidney index.

In the experiment on a rat model of renal ischemia-reperfusion (33) 3 days after magnetic targeting of adipose-derived EPCs, a 2.15-fold increase in cell concentration was observed in the left kidney (the right kidney was removed according to the model used). This was accompanied by a 2.46-fold and 2.06-fold reduction in serum urea nitrogen and creatinine levels, respectively. Additionally, apoptosis in the renal parenchyma decreased by 2.65-fold, while proliferative activity increased by 3.48-fold.

In all the reviewed models, the use of magnetic targeting significantly increased cell concentration in the target area, enhancing their retention and regenerative activity. This was reflected across various models in the expansion of tissue repair areas, thickening of the urethral sphincter, increased vascularization, and growth of myofibrous tissue. A reduction in inflammatory cytokine levels and tissue apoptosis was observed, along with improvements in functional outcomes.

Models of eye diseases

In a study using a glaucoma model developed with MYOC-Y437H transgenic mice (12) it was demonstrated that the injection of magnetically labeled trabecular meshwork cells (TMCs) derived from induced pluripotent stem cells (iPSCs) into the anterior chamber of the eye, combined with the application of a ring magnet (60 mT induction, 15-minute exposure), localized approximately 30% of the injected cells to the target area. This value exceeded the control group (no magnet) by 2.8–3.9 times. The cells were evenly distributed within the magnetic capture zone. Magnetic targeting was associated with a temporary reduction in intraocular pressure (IOP) over 10 days post-cell injection, with a maximum reduction of 8.8% on day 8. Regardless of magnetic targeting, cell therapy significantly reduced IOP by approximately 11–19% throughout the observation period (17 days).

Using a similar model of glaucoma (11) it was shown that the use of a cylindrical magnet with 0.25 T induction for magnetic targeting of MMSCs and TMCs led to a significant reduction in IOP. Specifically, the application of MMSCs resulted in a 27% reduction in IOP after 9

[Downloaded from mjiri.iums.ac.ir on 2026-10-14]

[DOI: 10.47176/mjiri.39.91]

months, while the application of TMCs led to a 13% reduction in IOP after 3–4 months post-cell injection.

In a rabbit model of corneal endothelial dysfunction (42) it was shown that magnetic targeting of corneal endothelial cells for 3 hours after their injection into the anterior chamber of the eye led to a 37% reduction in corneal edema after 7 days, compared to the control group without magnetic targeting. On day 14, a slight increase in corneal transparency was observed.

In the work on Chinchilla rabbits (43), the possibility of retaining MMSCs using a magnetic disk implant after subretinal cell injection was demonstrated. A progressive decrease in the fluorescent signal from magnetically labeled MMSCs (carrying the transgenic GFP) was observed over 9 days, probably indicating their elimination. The survival rate and number of retained cells were significantly influenced by the culturing conditions, particularly the oxygen level in the CO_2 incubator. MMSCs cultured in an atmosphere with 5% oxygen (hypoxia) showed significantly better survival compared to cells cultured under 21% oxygen concentration.

In the context of these diseases, it can be concluded that magnetic targeting improves the localization of administered cells to the target area, as confirmed in glaucoma and corneal endothelial dysfunction models. This approach enhances both short-term and long-term therapeutic effects of cell therapy, including reductions in IOP and corneal edema. Notably, a more pronounced and sustained decrease in IOP was observed in the glaucoma model with the use of MMSCs.

Models of ischemic heart disease

The use of magnetic retention of MSCs for 7 days after their intramyocardial injection in a mouse model of ischemia-reperfusion (18) led to an 11% and 21% increase in left ventricular ejection fraction (LVEF) on the 30th and 60th day, respectively. On day 60 of observation, a 43% reduction in cardiomegaly and a decrease in fibrosis levels were also noted.

The use of a dual-layer magnetic epicardial implant to retain magnetically labeled endothelial cells in a rat model of myocardial infarction (15) enhanced angiogenesis in the infarct zone on day 14. The implantation area of endothelial cells increased by 4.6 times, and tissue perfusion increased by 3.14 times. On day 28, improvements in the structural and functional state of the myocardium were observed, including increase of LVEF by 10%, decrease of infarct area by 38% and degree of fibrosis by 50%, as well as a 30% increase in myocardial wall thickness and a 32% increase in perfusion in the area of implant location.

In a similar rat myocardial infarction model (14) intravenous injection of bone marrow-derived EPCs, combined with magnetic targeting for 1 hour in the infarct zone, led to a 3-fold increase in cell concentration in the target area 4 weeks after administration. This was accompanied by an 11% increase in LVEF, a 35% reduction in infarct size, and a 29% reduction in myocardial apoptosis. Additionally, levels of collagen types I and III were reduced by 28% and 41% respectively, as well as TGFβ by 24%. In the infarct zone, an increase in microvascular density was observed, along with the expression of angiogenesis factors, including VEGF (48%), IGF-1 (31%), PDGF (27%), SDF-1α (28%), and βFGF (32%).

In the analyzed models of ischemic heart disease, the use of magnetic targeting significantly enhanced the localization and subsequent implantation of administered cells in the damaged myocardial zone. All studies reported a substantial increase in LVEF by 10–21%, depending on the cell type and observation duration, indicating the restoration of myocardial contractile function. Additionally, a deceleration of pathological cardiac remodeling processes was observed, including reductions in fibrosis, infarct size, cardiomegaly, and myocardial apoptosis. Magnetic targeting also promoted enhanced angiogenesis, as evidenced by improved tissue microcirculation and increased expression of angiogenic factors.

Cancer disease models

In a mouse model of lymphoma (cell line EG7-OVA) (35), magnetic targeting of intravenously administered cytotoxic T lymphocytes (CTLs) to the peritumoral area for 90 minutes resulted in a 2.17-fold increase in their concentration in tumor-draining lymph nodes after 14 days. There was a 21% reduction in tumor infiltration and a 2.03-fold increase in tumor volume compared to the group without magnetic targeting.

In another study on mice (24) with inoculated tumors of EG7 (lymphoma) and 4T1 (breast cancer) lines, magnetic targeting of CTLs or tumor-infiltrating lymphocytes (TILs) directly into the tumor for 12 hours resulted in a 3-fold enhancement of tumor infiltration by the injected cells. This led to complete tumor suppression and 100% survival of the animals during the 35-day observation period.

On the model of Sa-37 sarcoma in mice (44) magnetic targeting of DCs to the inguinal lymph nodes for 1 hour following intracutaneous cell administration resulted in a 45% reduction in tumor growth and a 31% reduction in tumor mass by day 28. Within the tumor tissue, a 3.5-fold decrease in TGF-β expression was observed, potentially indicating weakened tumor-driven immunosuppressive mechanisms. At the same time, a 5-fold increase in IL-10 and a 3-fold increase in VEGF levels suggested activation of anti-inflammatory and angiogenic processes that might support tumor growth and vascularization. In the lymph nodes, a 2-fold increase in IL-4 expression was recorded, indicative of a Th2 response that could promote immune tolerance, along with a 4.5-fold increase in INF-γ, signifying an enhancement of cellular immune responses and cytotoxic mechanisms. These changes in the cytokine landscape reflect a complex interaction between the activation of antitumor processes and tumor responses to counteract these mechanisms.

In a mouse model of implanted G422 brain glioma (29), magnetic targeting of neutrophils to the tumor site using a rotating magnetic field device with an induction of 5 mT and a frequency of 1 Hz for 1 hour increased the local concentration of cells within the tumor by 2.7-fold. In this study, neutrophils served as carriers for the anticancer drug paclitaxel. The use of magnetic targeting extended

[Downloaded from mjiri.iums.ac.ir on 2026-10-14]

[DOI: 10.47176/mjiri.39.91]

the animals' median survival time by 17% (to 35 days). When chemotactic agents for neutrophils were introduced into the tumor, the therapeutic effect of magnetic targeting was further enhanced, increasing the median survival time by 30% (to 43 days).

The presented data obtained from studies on various tumor models in mice highlight the potential of magnetic targeting of immune system cells. This approach enables a substantial increase in the local concentration of cells within tumors and associated lymph nodes, thereby enhancing the therapeutic efficacy of cancer immunotherapy. Additionally, it offers a promising strategy for targeted delivery of anti-cancer drugs using cells as a "living container."

Models of musculoskeletal disorders

In a mouse model of muscle inflammation (myositis) (20) the use of a permanent magnet for 3 hours following intramuscular administration of magnetically labeled MMSCs resulted in a 2-fold increase in their local concentration 6 hours post-injection. After 5 days, the muscles exhibited a reduction in the expression of pro-inflammatory cytokines TNF-α by 1.9-fold and IL-1β by 3.1-fold, along with an increase in IL-6 levels by 2.3-fold and IL-10 levels by 1.5-fold, indicating the activation of anti-inflammatory mechanisms.

Magnetic targeting was also used in a study on osteoarthritis in rabbits (16). Retention of magnetically labeled chondrocytes within the knee joint capsule using a magnetic field for 8 weeks increased proteoglycan secretion levels by 51% in the cartilage damage zone compared to the control group without magnetic targeting. This indicates the activation of cartilage matrix synthesis and secretion processes, contributing to cartilage tissue repair and improving joint condition in osteoarthritis.

The presented data demonstrate the effectiveness of magnetic targeting in enhancing the therapeutic impact of cell therapy for various musculoskeletal disorders.

Other disease models

An experiment using a model of endothelial layer injury of the carotid artery (induced by balloon catheter compression) (25) demonstrated a 20-fold retention of MMSCs in the target area 5 minutes after applying a magnetic trap. Twenty-four hours after magnetic targeting, the MMSCs concentration in the injury site remained 5 times higher compared to the control group.

Magnetic targeting of MMSCs for 48 hours following intravenous administration in a mouse model of pulmonary silicosis (34) increased the local cell concentration in the lungs by 3.8-fold. This resulted in a 29% reduction in lung static elastance, a 60% decrease in resistive pressure, a 36% reduction in granuloma area, and a 50% decrease in IL-1β levels in lung tissue. These findings indicate a reduction in inflammatory and fibrotic processes, along with the restoration of lung tissue structure and function.

In the study of full-thickness skin burns in rats (54), magnetic targeting of MMSCs for 30 minutes at the wound site following intravenous administration enhanced MMSC persistence at the defect area 7 days post-injection. This was accompanied by a 21% increase in serum VEGF levels and a 25% reduction in IL-6, IL-1α, and IL-2 levels, indicating the activation of angiogenesis and anti-inflammatory processes. Notably, all experimental groups that received MMSCs demonstrated localized anti-inflammatory effects to varying degrees.

In a model of streptozotocin-induced diabetes in rats (55), magnetic targeting of MMSCs for 30 minutes following intravenous cell administration resulted in a 38% increase in local MMSC concentration in the pancreas two weeks later. Three weeks later, a higher level of β-cell preservation and a 34% reduction in β-cell apoptosis were observed compared to control animals, along with a 48% higher serum C-peptide level.

Risk of bias assessment results

Risk of bias results for individual studies are presented in Table 3.

Selection bias: Most studies (32/39) reported adequate randomization methods (Low risk), but seven studies lacked clarity (Unclear risk). Fourteen studies confirmed group similarity at baseline (Low risk), while 25 did not provide sufficient details (Unclear risk). No one has explicitly described concealment methods (Unclear risk).

Performance bias: No studies reported randomization of cage placement (Unclear risk). Only two studies ensured that caregivers/investigators were blinded (Low risk), but 37 failed to report it (Unclear risk).

Detection bias: No studies described random selection of animals for measurements (Unclear risk). Thirty-seven studies reported blinded assessors (Low risk), while 2 lacked details (Unclear risk).

Attrition bias: Thirty studies addressed missing data (Low risk), but 9 had Unclear reporting.

Reporting bias: Thirty-eight studies reported all pre-specified outcomes (Low risk); but 1 study (Wang Y. et al., 2022) showed High risk due to the preprint version of the article.

Other bias: All studies were rated Low risk, indicating no major confounding biases.

The bias assessment indicates that while most studies adequately addressed randomization, blinded outcome assessment, and complete outcome reporting, several critical methodological shortcomings persist. Notably, the failure to report baseline group characteristics, allocation concealment procedures, and caregiver/investigator blinding introduces significant risks of selection and performance bias. Furthermore, the absence of documented cage randomization methods and insufficient description of blinding protocols for personnel involved in animal care and experimentation further compromises the studies' internal validity. These reporting gaps highlight the need for greater methodological transparency in future research to ensure proper assessment and mitigation of potential biases across all experimental stages. The overall findings suggest that while core aspects of study design were generally well-executed, systematic improvements in documenting and implementing blinding protocols, allocation concealment, and environmental control measures are essential to strengthen the reliability of experimental outcomes.

[Downloaded from mjiri.iums.ac.ir on 2026-10-14]

[DOI: 10.47176/mjiri.39.91]

Table 3. Risk of bias results for individual studies (SYRCLE risk of bias tool)

Study reference	Selection bias (sequence generation)	Selection bias (baseline characteristics)	Selection bias (allocation concealment)	Performance bias (random housing)	Performance bias (blinding)	Detection bias (random outcome assessment)	Detection bias (blinding)	Attrition bias (incomplete outcome data)	Reporting bias (selective outcome reporting)	Other bias
Soto P.A. et al., 2021 (46)	Low	Low	Unclear	Unclear	Low	Unclear	Low	Low	Low	Low
Sun C. et al., 2021a (48)	Low	Low	Unclear	Unclear	Unclear	Unclear	Low	Low	Low	Low
Jin Y. et al., 2022 (47)	Unclear	Low	Unclear	Unclear	Unclear	Unclear	Low	Low	Low	Low
Sun C. et al., 2021b (17)	Low	Low	Unclear	Unclear	Low	Unclear	Low	Low	Low	Low
Yan J. et al., 2023 (49)	Low	Unclear	Unclear	Unclear	Unclear	Unclear	Low	Low	Low	Low
Kang M.K. et al., 2020 (19)	Low	Unclear	Unclear	Unclear	Unclear	Unclear	Low	Unclear	Low	Low
Zhang B. et al., 2020 (25)	Low	Unclear	Unclear	Unclear	Unclear	Unclear	Low	Unclear	Low	Low
El-Latif N.A. et al., 2024 (28)	Low	Low	Unclear	Unclear	Unclear	Unclear	Low	Low	Low	Low
Wang Y. et al., 2022 (50)	Low	Unclear	Unclear	Unclear	Unclear	Unclear	Low	Low	High	Low
Hour F.Q. et al., 2020 (39)	Low	Unclear	Unclear	Unclear	Unclear	Unclear	Low	Unclear	Low	Low
Jung M. et al., 2023 (22)	Low	Unclear	Unclear	Unclear	Unclear	Unclear	Low	Low	Low	Low
Moayeri A. et al., 2020 (51)	Low	Unclear	Unclear	Unclear	Unclear	Unclear	Low	Low	Low	Low
Simorgh S. et al., 2021 (40)	Low	Low	Unclear	Unclear	Unclear	Unclear	Low	Low	Low	Low
Jeon S. et al., 2021 (38)	Low	Unclear	Unclear	Unclear	Unclear	Unclear	Low	Low	Low	Low
Sadahide K. et al., 2019 (45)	Unclear	Unclear	Unclear	Unclear	Unclear	Unclear	Low	Low	Low	Low
Wang Y. et al., 2020 (52)	Low	Unclear	Unclear	Unclear	Unclear	Unclear	Low	Low	Low	Low

[Downloaded from mjiri.iums.ac.ir on 2026-10-14]

[DOI: 10.47176/mjiri.39.91]

Table 3. Risk of bias results for individual studies (SYRCLE risk of bias tool)

Study reference	Selection bias (sequence generation)	Selection bias (baseline characteristics)	Selection bias (allocation concealment)	Performance bias (random housing)	Performance bias (blinding)	Detection bias (random outcome assessment)	Detection bias (blinding)	Attrition bias (incomplete outcome data)	Reporting bias (selective outcome reporting)	Other bias
Wang K. et al., 2024 (53)	Low	Unclear	Unclear	Unclear	Unclear	Unclear	Low	Low	Low	Low
Wu D. et al., 2023 (33)	Low	Unclear	Unclear	Unclear	Unclear	Unclear	Low	Low	Low	Low
Wang X. et al., 2022 (12)	Low	Unclear	Unclear	Unclear	Unclear	Unclear	Low	Low	Low	Low
Xia X. et al., 2019 (42)	Low	Unclear	Unclear	Unclear	Unclear	Unclear	Low	Low	Low	Low
Fard M.R.B. et al., 2024 (11)	Low	Low	Unclear	Unclear	Unclear	Unclear	Low	Low	Low	Low
Plakhotniy M.A. et al., 2020 (43)	Unclear	Unclear	Unclear	Unclear	Unclear	Unclear	Low	Unclear	Low	Low
Chen F. et al., 2019 (18)	Low	Unclear	Unclear	Unclear	Unclear	Unclear	Low	Low	Low	Low
Qian B. et al., 2023 (15)	Low	Unclear	Unclear	Unclear	Unclear	Unclear	Low	Unclear	Low	Low
Zhang B.F. et al., 2019 (14)	Low	Unclear	Unclear	Unclear	Unclear	Unclear	Low	Unclear	Low	Low
Sanz-Ortega L. et al., 2019a (35)	Low	Low	Unclear	Unclear	Unclear	Unclear	Low	Unclear	Low	Low
Nie W. et al., 2019 (24)	Low	Low	Unclear	Unclear	Unclear	Unclear	Low	Low	Low	Low
Khranovska N. et al., 2021 (44)	Low	Low	Unclear	Unclear	Unclear	Unclear	Low	Low	Low	Low
Zhang H. et al., 2021 (29)	Unclear	Unclear	Unclear	Unclear	Unclear	Unclear	Unclear	Unclear	Low	Low
Kono Y. et al., 2021a (20)	Unclear	Unclear	Unclear	Unclear	Unclear	Unclear	Low	Low	Low	Low

[Downloaded from mjiri.iums.ac.ir on 2026-10-14]

[DOI: 10.47176/mjiri.39.91]

Table 3. Risk of bias results for individual studies (SYRCLE risk of bias tool)

Study reference	Selection bias (sequence generation)	Selection bias (baseline characteristics)	Selection bias (allocation concealment)	Performance bias (random housing)	Performance bias (blinding)	Detection bias (random outcome assessment)	Detection bias (blinding)	Attrition bias (incomplete outcome data)	Reporting bias (selective outcome reporting)	Other bias
Yang S.W. et al., 2022 (16)	Unclear	Unclear	Unclear	Unclear	Unclear	Unclear	Low	Low	Low	Low
Silva L.H.A. et al., 2020 (34)	Low	Low	Unclear	Unclear	Unclear	Unclear	Low	Low	Low	Low
Ahn Y.J. et al., 2021 (13)	Low	Low	Unclear	Unclear	Unclear	Unclear	Unclear	Low	Low	Low
Li X. et al., 2020a (54)	Low	Unclear	Unclear	Unclear	Unclear	Unclear	Low	Low	Low	Low
Li X. et al., 2020b (55)	Low	Unclear	Unclear	Unclear	Unclear	Unclear	Low	Low	Low	Low
Sanz-Ortega L. et al., 2019b (36)	Low	Low	Unclear	Unclear	Unclear	Unclear	Low	Unclear	Low	Low
Cai Q. et al., 2020 (41)	Low	Unclear	Unclear	Unclear	Unclear	Unclear	Low	Low	Low	Low
Harrison R. et al., 2019 (37)	Low	Low	Unclear	Unclear	Unclear	Unclear	Low	Low	Low	Low
Kono Y. et al., 2021b (23)	Unclear	Unclear	Unclear	Unclear	Unclear	Unclear	Low	Low	Low	Low

[Downloaded from mjiri.iums.ac.ir on 2026-10-14]

[DOI: 10.47176/mjiri.39.91]

Discussion

According to data from the PubMed portal, the number of publications related to the use of magnetic particles in biomedical research has been steadily increasing annually. Most studies in this field over the past 5 years have focused on magnetically guided drug delivery (56), hyperthermia cancer therapy (57), MRI contrast enhancement (including in the context of cell therapy) (58, 59), and magnetic separation of cells (60). In contrast, significantly fewer studies have explored magnetic delivery and/or retention of cells in target zones, the use of magnetic cell labeling in tissue engineering (including magnetic assembly of spheroids (61) and tissue equivalents (62)), magnetic stimulation of cells (63) or the application of various sizes and designs of magnetic cell carriers (such as magnetic spheres, spirals and "microbots") (64).

Specialists in regenerative medicine are well aware of one of the primary obstacles to the widespread clinical adoption of cell therapy, including the use of stem cells – its low clinical efficacy (65, 66). For instance, according to data from clinicaltrials.gov, a search for "mesenchymal stem cells" as of November 2024 yields 1702 registered clinical trials, of which 583 are completed. However, as of 2023, only 12 cell-based medicinal products utilizing MMSCs have been officially registered worldwide (67). Among the main reasons for the low clinical efficacy of cell therapy is the insufficient local concentration of cells introduced into the body, attributed to ineffective homing, the pathological state of the target tissue, physiological characteristics of the target zone, and other factors.

In certain cases, this issue can be addressed by using magnetic targeting and/or retention of cells introduced into the body that have been labeled with magnetic particles. Despite the relatively limited number of studies focusing on magnetic cell targeting (we identified 39 studies out of nearly 11000 published over the past 5 years), we believe their importance is significant, as they demonstrate the potential for this approach to increase the efficiency of cell therapy. According to the data from the reviewed studies, magnetic targeting has significantly (ranging from 1.16 up to 20 times) increased the local concentration of cells delivered into the body (Figure 3), resulting in more pronounced therapeutic effects in nearly all animal disease models (with the exception of one study (28)) compared to conditions where magnetic targeting was not employed. This underscores the considerable therapeutic potential of magnetic targeting in cell therapy.

It is worth noting that no clinical studies were identified during the analyzed period, although limited clinical trials were conducted in earlier years. For instance, in Japan in 2018, magnetic targeting of autologous MMSCs was applied following intra-articular administration to five patients with osteoarthritis (68). Significant improvement in cartilage tissue condition was observed, with no complications reported during the 48-week follow-up period.

Among the targets for magnetic guidance, three groups of cells are of greatest interest: MMSCs (59% of studies), immune cells (18%), and endothelial cells with their progenitors (18%). This distribution reflects their clinical relevance and potential application in various diseases. Specifically, MMSCs can be used both for repairing mesenchymal tissue defects and for treating autoimmune diseases, chronic inflammatory conditions, and ischemic tissue injuries due to their paracrine effects, which include anti-inflammatory, immunosuppressive, angiogenic, and anti-apoptotic actions (69). The clinical potential of endothelial cells and EPCs lies in the treatment of vascular disorders and ischemic conditions (70, 71), while immune cells show promise for cancer immunotherapy (72).

A significant portion of disease models involved disorders of the nervous system, primarily various types of brain ischemic injuries and neurodegenerative diseases, with the use of MMSCs. The rationale for applying magnetic targeting in this group of diseases is likely associated with the difficulty of delivering cells to the affected tissue due to the presence of the skull and the blood-brain barrier. Another notable group includes cancer models (various types of implanted tumors) employing immune cells, such as T-lymphocytes, DCs, and neutrophils. Magnetic targeting in this group aims to overcome tumor-associated barriers (physical, receptor, and cytokine-related), thereby enhancing tumor infiltration by immune cells (or their localization in tumor-draining lymph nodes, as in the case of DCs) and facilitating tumor elimination. In models of eye diseases and ischemic heart injuries, MMSCs, endothelial cells, and EPCs were used equally. In the case of eye diseases, magnetic targeting ensures precise localization of cells within the anatomically complex structure of the eye. For ischemic heart injuries, it enables retention of locally delivered cells on the actively functioning and highly perfused organ.

Regarding the choice of labeling agents in the analyzed studies, a certain consensus has emerged: the use of materials whose magnetic core consists of nano- or microscale iron oxide particles (SPIONs or MPIO). The preference for these types of particles is due to their combination of superparamagnetic properties, allowing magnetization only under an external magnetic field without hysteresis, along with relatively low cytotoxicity and biodegradability. Following exocytosis or the death of labeled cells, these magnetic particles are processed by the reticuloendothelial system of the body, replenishing the body's natural iron reserves (73). Magnetic particle shells demonstrate considerable diversity (represented by 18 distinct types), indicating that this component is the focus of scientific research. Shell composition appeared to influence cell viability and functionality. For example, SPIONs with poly-L-lysine coatings were associated with oxidative stress in one study (28), whereas dextran-coated particles demonstrated better biocompatibility (39).

In the majority of cases (77%), magnetic particles with a negative charge were used, which might initially seem a counterintuitive choice given the negative charge of the cell membrane. A possible explanation for this lies in the interaction of magnetic particles with proteins or other components of the medium that neutralize their negative charge, thereby facilitating their uptake by cells. Interaction with cell membrane proteins is also possible. For instance, Zhao F. et al. (74) demonstrated in their study that negatively charged nanoparticles enter cells through cave-

[Downloaded from mjiri.iums.ac.ir on 2026-10-14]

[DOI: 10.47176/mjiri.39.91]

olin- and/or clathrin-mediated endocytosis. It may be suggested that protein corona formation or endocytic pathways could potentially override or modulate electrostatic interactions. Furthermore, negatively charged magnetic particles may help prevent excessive cell labeling with magnetic particles and reduce cytotoxicity.

While our systematic review highlights the efficacy of magnetic cell targeting in preclinical models, several limitations must be acknowledged. First, the incomplete coverage of bibliographic databases. The study was conducted using PubMed, Cochrane Library, and eLibrary, but databases such as Scopus, Web of Science, and Google Scholar were not used. Additionally, a significant portion of the studies that met the inclusion criteria (20 studies) were not available in full-text versions for detailed analysis. Furthermore, the selected studies presented incomplete data. For instance, the charge of the magnetic particles was reported in 19 out of 39 studies; 6 articles did not include information on the stabilizing coating, and three studies lacked data on the optimal labeling concentration of the magnetic particles.

Second, the high heterogeneity in study designs – including variations in animal models, cell types, magnetic particle formulations, and outcome measures – complicates direct comparisons and meta-analyses. For instance, differences in magnetic field strength (0.005 – 1.45 T) and particle size (10 nm – 2.8 μm) across studies may influence capture efficiency and therapeutic outcomes, yet our correlation analysis (data not shown) revealed no significant associations, likely due to methodological disparities. Second, only 19 of 39 studies provided quantitative data on cell retention, underscoring a need for standardized reporting in future work.

Third, the predominance of small-animal models (e.g., rodents) raises concerns about the generalizability of findings to larger animals or humans (75, 76), where anatomical and physiological barriers (e.g., deeper target tissues, higher blood flow rates) may reduce targeting efficacy. The nonlinear decay of magnetic field strength with distance limits the effective range of permanent magnets (77), which are optimized for small-animal anatomy but may fail to retain cells in deeper human tissues. According to data from our research group (78), the capture distance of magnetically labelled fibroblasts using a disc-shaped neodymium magnet with a magnetic field strength of 0.255 T did not exceed 3-4 mm. This is consistent with the general limitations observed in magnetic targeting. Electromagnets or implantable devices (e.g., epicardial patches (15)) could address this, yet their safety and scalability require further validation.

Additionally, while SPIONs showed favorable biocompatibility in animal studies, their long-term fate in humans, including potential iron accumulation and immune responses, remains understudied. Regulatory hurdles, such as defining acceptable iron loads and labeling protocols, further complicate clinical adoption. Future studies should prioritize large-animal models (e.g., pigs) to bridge this translational gap.

In general, current magnetic targeting technology is constrained by the trade-off between field strength and tissue penetration. While neodymium magnets achieve high gradients (>1 T), their static nature limits adaptability to dynamic physiological environments. Emerging solutions include pulsed electromagnetic fields (29) and magnetically guided microrobots (64), which offer spatiotemporal control but require miniaturization and real-time imaging integration. Another limitation is the lack of non-invasive, high-resolution tools to track magnetically labeled cells in vivo over prolonged periods. Advances in MRI contrast agents or hybrid imaging modalities (e.g., MPI-MRI) could address this gap (59).

One potential advancement in magnetic cell targeting could be the use of Digital Twin technology – computational models that simulate individual patient anatomy and physiology (79). This approach may revolutionize magnetic targeting by enabling personalized optimization of parameters (e.g., magnet placement, magnetic field exposition time) prior to intervention. For example, patient-specific vascular models could predict cell capture efficiency under flow conditions, while machine learning might analyze historical data to correlate particle properties with therapeutic outcomes. While these strategies could minimize trial-and-error inefficiencies in clinical translation, key challenges persist, including the automated generation of patient-specific models and the need for rigorous experimental validation (80, 81).

In summary, while magnetic cell targeting holds significant promise for enhancing cell therapy, its clinical translation requires addressing heterogeneity in preclinical studies, technological limitations, and biological variability. Collaborative efforts to standardize protocols, validate large-animal models, and integrate innovative tools (e.g., digital twins) will be critical to realizing this potential.

Conclusion

Magnetic targeting of cells in the field of cell therapy represents an actively developing area within regenerative medicine. Among the experimental studies on animal disease models conducted over the last 5 years, a significant proportion focused on diseases of the nervous system, heart, eyes, urinary system, musculoskeletal system, oncology, and other conditions. The most commonly labeled cells were MMSCs, endothelial cells, EPCs, T-cells, macrophages, neutrophils, chondrocytes, myoblasts, neural progenitors, and erythrocytes. Superparamagnetic nano- or microscale iron oxide particles were used for magnetic labeling in all studies, and permanent magnets, primarily neodymium magnets, were used as magnetic traps.

In animal model studies, magnetic targeting has shown, in most cases, a manyfold increase in the local concentration of introduced cells, resulting in more pronounced therapeutic effects compared to control groups without magnetic targeting. This demonstrates the high clinical potential of this approach in cell therapy.

In conclusion, while magnetic cell targeting demonstrates considerable preclinical promise, its clinical translation hinges on overcoming key challenges – including study heterogeneity, technological limitations in field penetration and cell tracking, and unresolved biocompatibility concerns. Given these barriers, future studies should prior-

[Downloaded from mjiri.iums.ac.ir on 2026-10-14]

[DOI: 10.47176/mjiri.39.91]

itize transitioning from small animal models (e.g., rodents) to large-animal models (e.g., pigs, dogs) to better approximate human physiology and facilitate eventual clinical trials. Further efforts must also focus on standardizing protocols, validating targeting efficacy in these advanced models, and integrating innovative tools such as digital twins to optimize personalized parameters. Together, these steps will be critical for bridging the gap between benchtop research and clinical application.

Authors' Contributions

All authors contributed to the development of the study concept and design, but the primary idea of the study belongs to Svetlana Bespalova and Yuri Legenkiy. Viktor Turchin, Maxim Solopov, and Yuri Legenkiy were responsible for data management, primary evaluation, and interpretation of the results. Viktor Turchin drafted the manuscript. Roman Ishchenko, Svetlana Bespalova, Mikhail Kiselevskiy, and Andrey Popandopulo critically reviewed and revised the draft, provided final edits, and approved the version for publication.

Ethical Considerations

Not applicable.

Acknowledgment

The support provided by the Department of Physics of Magnetic Phenomena and High-Temperature Superconductivity, Donetsk State University, to conduct this study is highly acknowledged.

Conflict of Interests

The authors declare that they have no competing interests.

References

1. Van den Bos J, Ouaamari YE, Wouters K, Cools N, Wens I. Are Cell-Based Therapies Safe and Effective in the Treatment of Neurodegenerative Diseases? A Systematic Review with Meta-Analysis. Biomolecules. 2022 Feb 21;12(2):340.
2. Fan Y, Goh ELK, Chan JKY. Neural Cells for Neurodegenerative Diseases in Clinical Trials. Stem Cells Transl Med. 2023 Aug 16;12(8):510–26.
3. Sordi V, Monaco L, Piemonti L. Cell Therapy for Type 1 Diabetes: From Islet Transplantation to Stem Cells. Horm Res Paediatr. 2023;96(6):658–69.
4. Montoto-Meijide R, Meijide-Faílde R, Díaz-Prado SM, Montoto-Marqués A. Mesenchymal Stem Cell Therapy in Traumatic Spinal Cord Injury: A Systematic Review. Int J Mol Sci. 2023 Jul 20;24(14):11719.
5. Wu KC, Chang YH, Ding DC, Lin SZ. Mesenchymal Stromal Cells for Aging Cartilage Regeneration: A Review. Int J Mol Sci. 2024 Nov 30;25(23):12911.
6. Michalska N, Totoń E, Kopczyński P, Jankowska-Wajda M, Rubiś B. Alternative Therapies in Transplantology as a Promising Perspective in Medicine. Ann Transplant. 2024 Jun 4;29:e943387.
7. Iansante V, Chandrashekran A, Dhawan A. Cell-based liver therapies: past, present and future. Philos Trans R Soc Lond B Biol Sci. 2018 Jul 5;373(1750):20170229.
8. Yun CW, Lee SH. Potential and Therapeutic Efficacy of Cell-based Therapy Using Mesenchymal Stem Cells for Acute/chronic Kidney Disease. Int J Mol Sci. 2019 Apr 1;20(7):1619.
9. Yun CW, Lee SH. Enhancement of Functionality and Therapeutic Efficacy of Cell-Based Therapy Using Mesenchymal Stem Cells for Cardiovascular Disease. Int J Mol Sci. 2019 Feb 24;20(4):982.
10. Achón Buil B, Tackenberg C, Rust R. Editing a gateway for cell therapy across the blood-brain barrier. Brain J Neurol. 2023 Mar 1;146(3):823–41.
11. Fard MRB, Chan J, Read AT, Li G, Cheng L, Safa BN, et al. Magnetically Steered Cell Therapy For Functional Restoration Of Intraocular Pressure Control In Open-Angle Glaucoma. BioRxiv Prepr Serv Biol. 2024 May 15;2024.05.13.593917.
12. Wang X, Cao Q, Wu S, Bahrani Fard MR, Wang N, Cao J, et al. Magnetic Nano-Platform Enhanced iPSC-Derived Trabecular Meshwork Delivery and Tracking Efficiency. Int J Nanomedicine. 2022;17:1285–307.
13. Ahn YJ, Yun WS, Choi JS, Kim WC, Lee SH, Park DJ, et al. Biodistribution of poly clustered superparamagnetic iron oxide nanoparticle labeled mesenchymal stem cells in aminoglycoside induced ototoxic mouse model. Biomed Eng Lett. 2021 Feb;11(1):39–53.
14. Zhang BF, Jiang H, Chen J, Hu Q, Yang S, Liu XP. Silica-coated magnetic nanoparticles labeled endothelial progenitor cells alleviate ischemic myocardial injury and improve long-term cardiac function with magnetic field guidance in rats with myocardial infarction. J Cell Physiol. 2019 Aug;234(10):18544–59.
15. Qian B, Shen A, Huang S, Shi H, Long Q, Zhong Y, et al. An Intrinsically Magnetic Epicardial Patch for Rapid Vascular Reconstruction and Drug Delivery. Adv Sci Weinh Baden-Wurtt Ger. 2023 Dec;10(36):e2303033.
16. Yang SW, Chen YJ, Chen CJ, Liu JT, Yang CY, Tsai JH, et al. High-Density Horizontal Stacking of Chondrocytes via the Synergy of Biocompatible Magnetic Gelatin Nanocarriers and Internal Magnetic Navigation for Enhancing Cartilage Repair. Polymers. 2022 Feb 19;14(4):809.
17. Sun C, Zou N, Chen H, Zhang A, Sun L, Liu Z, et al. The effect of magnetic guiding BMSCs on hypoxic-ischemic brain damage via magnetic resonance imaging evaluation. Magn Reson Imaging. 2021 Jun;79:59–65.
18. Chen F, Zhao ER, Hableel G, Hu T, Kim T, Li J, et al. Increasing the Efficacy of Stem Cell Therapy via Triple-Function Inorganic Nanoparticles. ACS Nano. 2019 Jun 25;13(6):6605–17.
19. Kang MK, Kim TJ, Kim YJ, Kang L, Kim J, Lee N, et al. Targeted Delivery of Iron Oxide Nanoparticle-Loaded Human Embryonic Stem Cell-Derived Spherical Neural Masses for Treating Intracerebral Hemorrhage. Int J Mol Sci. 2020 May 22;21(10):3658.
20. Kono Y, Takegaki J, Ohba T, Matsuda K, Negoro R, Fujita S, et al. Magnetization of mesenchymal stem cells using magnetic liposomes enhances their retention and immunomodulatory efficacy in mouse inflamed skeletal muscle. Int J Pharm. 2021 Mar 1;596:120298.
21. Devine SM, Cobbs C, Jennings M, Bartholomew A, Hoffman R. Mesenchymal stem cells distribute to a wide range of tissues following systemic infusion into nonhuman primates. Blood. 2003 Apr 15;101(8):2999–3001.
22. Jung M, Kim H, Hwang JW, Choi Y, Kang M, Kim C, et al. Iron Oxide Nanoparticle-Incorporated Mesenchymal Stem Cells for Alzheimer's Disease Treatment. Nano Lett. 2023 Jan 25;23(2):476–90.
23. Kono Y, Gogatsubo S, Ohba T, Fujita T. Enhanced macrophage delivery to the colon using magnetic lipoplexes with a magnetic field. Drug Deliv. 2019 Dec;26(1):935–43.
24. Nie W, Wei W, Zuo L, Lv C, Zhang F, Lu GH, et al. Magnetic Nanoclusters Armed with Responsive PD-1 Antibody Synergistically Improved Adoptive T-Cell Therapy for Solid Tumors. ACS Nano. 2019 Feb 26;13(2):1469–78.
25. Zhang B, Mo X, Yu F, Ma Y, Yan F. Ultrasound monitoring of magnet-guided delivery of mesenchymal stem cells labeled with magnetic lipid-polymer hybrid nanobubbles. Biomater Sci. 2020 Jul 7;8(13):3628–39.
26. Pai A, Cao P, White EE, Hong B, Pailevanian T, Wang M, et al. Dynamically Programmable Magnetic Fields for Controlled Movement of Cells Loaded with Iron Oxide Nanoparticles. ACS Appl Bio Mater. 2020 Jul 20;3(7):4139–47.
27. Gong X, Wang F, Huang Y, Lin X, Chen C, Wang F, et al. Magnetic-targeting of polyethylenimine-wrapped iron oxide nanoparticle labeled chondrocytes in a rabbit articular cartilage defect model. RSC Adv. 2018 Feb 14;8(14):7633–40.
28. El-Latif NA, El Zehary RR, Ibrahim FM, Denewar M. Bone marrow stem cells with or without superparamagnetic iron oxide nanoparticles as a magnetic targeting tool: Which is better in regeneration of neurolysed facial nerve? An experimental study. Heliyon. 2024 Feb

[Downloaded from mjiri.iums.ac.ir on 2026-10-14]

[DOI: 10.47176/mjiri.39.91]

29;10(4):e26675.
29. Zhang H, Li Z, Gao C, Fan X, Pang Y, Li T, et al. Dual-responsive biohybrid neutrobots for active target delivery. Sci Robot. 2021 Mar 24;6(52):eaaz9519.
30. Ahn YJ, Kong TH, Choi JS, Yun WS, Key J, Seo YJ. Strategies to enhance efficacy of SPION-labeled stem cell homing by magnetic attraction: a systemic review with meta-analysis. Int J Nanomedicine. 2019;14:4849–66.
31. Page MJ, McKenzie JE, Bossuyt PM, Boutron I, Hoffmann TC, Mulrow CD, et al. The PRISMA 2020 statement: an updated guideline for reporting systematic reviews. The BMJ. 2021 Mar 29;372:n71.
32. Hooijmans CR, Rovers MM, de Vries RBM, Leenaars M, Ritskes-Hoitinga M, Langendam MW. SYRCLE's risk of bias tool for animal studies. BMC Med Res Methodol. 2014 Mar 26;14:43.
33. Wu D, Liu J, Zhou C, Ma W, Zhou L, Ge Y, et al. Immunomagnetic Delivery of Adipose-Derived Endothelial Progenitor Cells for the Repair of Renal Ischemia-Reperfusion Injury in a Rat Model. Bioeng Basel Switz. 2023 Apr 24;10(5):509.
34. Silva LHA, Silva MC, Vieira JB, Lima ECD, Silva RC, Weiss DJ, et al. Magnetic targeting increases mesenchymal stromal cell retention in lungs and enhances beneficial effects on pulmonary damage in experimental silicosis. Stem Cells Transl Med. 2020 Oct;9(10):1244–56.
35. Sanz-Ortega L, Portilla Y, Pérez-Yagüe S, Barber DF. Magnetic targeting of adoptively transferred tumour-specific nanoparticle-loaded CD8+ T cells does not improve their tumour infiltration in a mouse model of cancer but promotes the retention of these cells in tumour-draining lymph nodes. J Nanobiotechnology. 2019 Aug 6;17(1):87.
36. Sanz-Ortega L, Rojas JM, Marcos A, Portilla Y, Stein JV, Barber DF. T cells loaded with magnetic nanoparticles are retained in peripheral lymph nodes by the application of a magnetic field. J Nanobiotechnology. 2019 Jan 22;17(1):14.
37. Harrison R, Luckett J, Marsh S, Lugo Leija HA, Salih S, Alkharji R, et al. Magnetically Assisted Control of Stem Cells Applied in 2D, 3D and In Situ Models of Cell Migration. Mol Basel Switz. 2019 Apr 19;24(8):1563.
38. Jeon S, Park SH, Kim E, Kim JY, Kim SW, Choi H. A Magnetically Powered Stem Cell-Based Microrobot for Minimally Invasive Stem Cell Delivery via the Intranasal Pathway in a Mouse Brain. Adv Healthc Mater. 2021 Oct;10(19):e2100801.
39. Hour FQ, Moghadam AJ, Shakeri-Zadeh A, Bakhtiyari M, Shabani R, Mehdizadeh M. Magnetic targeted delivery of the SPIONs-labeled mesenchymal stem cells derived from human Wharton's jelly in Alzheimer's rat models. J Control Release Off J Control Release Soc. 2020 May 10;321:430–41.
40. Simorgh S, Bagher Z, Farhadi M, Kamrava SK, Boroujeni ME, Namjoo Z, et al. Magnetic Targeting of Human Olfactory Mucosa Stem Cells Following Intranasal Administration: a Novel Approach to Parkinson's Disease Treatment. Mol Neurobiol. 2021 Aug;58(8):3835–47.
41. Cai Q, Mai X, Miao W, Zhou X, Zhang Y, Liu X, et al. Specific, Non-Invasive, and Magnetically Directed Targeting of Magnetic Erythrocytes in Blood Vessels of Mice. IEEE Trans Biomed Eng. 2020 Aug;67(8):2276–85.
42. Xia X, Atkins M, Dalal R, Kuzmenko O, Chang KC, Sun CB, et al. Magnetic Human Corneal Endothelial Cell Transplant: Delivery, Retention, and Short-Term Efficacy. Invest Ophthalmol Vis Sci. 2019 Jun 3;60(7):2438–48.
43. Plakhotniy MA, Kodunov AM, Gorina EV, Boyarintsev VV, Trofimenko AV, Biryukov SA, et al. The effect of the cultivation conditions of mesenchymal stem cells on their viability upon being transplanted into the subretinal space (In Russian). Biophysics. 2020;65(6):1126–34.
44. Khranovska N, Skachkova O, Gorbach O, Inomistova M, Orel V. Magnetically sensitive nanocomplex enhances antitumor efficacy of dendritic cell-based immunotherapy. Exp Oncol. 2021 Sep;43(3):217–23.
45. Sadahide K, Teishima J, Inoue S, Tamura T, Kamei N, Adachi N, et al. Endoscopic repair of the urinary bladder with magnetically labeled mesenchymal stem cells: Preliminary report. Regen Ther. 2019 Jun;10:46–53.
46. Soto PA, Vence M, Piñero GM, Coral DF, Usach V, Muraca D, et al. Sciatic nerve regeneration after traumatic injury using magnetic targeted adipose-derived mesenchymal stem cells. Acta Biomater. 2021 Aug;130:234–47.
47. Jin Y, Shi P, Wang Y, Li J, Zhang J, Zhao X, et al. Precise control of embolic stroke with magnetized red blood cells in mice. Commun Biol. 2022 Feb 16;5(1):136.
48. Sun C, Zhang AD, Chen HH, Bian J, Liu ZJ. Magnet-targeted delivery of bone marrow-derived mesenchymal stem cells improves therapeutic efficacy following hypoxic-ischemic brain injury. Neural Regen Res. 2021 Nov;16(11):2324–9.
49. Yan J, Liu T, Li Y, Zhang J, Shi B, Zhang F, et al. Effects of magnetically targeted iron oxide@polydopamine-labeled human umbilical cord mesenchymal stem cells in cerebral infarction in mice. Aging. 2023 Feb 28;15(4):1130–42.
50. Wang Y, Jiang J, Fu X, Zhang J, Song J, Wang Y, et al. Fe3O4@polydopamine nanoparticle-loaded human umbilical cord mesenchymal stem cells improve the cognitive function in Alzheimer's disease mice by promoting hippocampal neurogenesis. Nanomedicine Nanotechnol Biol Med. 2022 Feb;40:102507.
51. Moayeri A, Darvishi M, Amraei M. Homing of Super Paramagnetic Iron Oxide Nanoparticles (SPIONs) Labeled Adipose-Derived Stem Cells by Magnetic Attraction in a Rat Model of Parkinson's Disease. Int J Nanomedicine. 2020;15:1297–308.
52. Wang Y, Zhou S, Yang R, Rahman M, Sequeira RC, Cao N, et al. Magnetic targeting of super-paramagnetic iron oxide nanoparticle labeled myogenic-induced adipose-derived stem cells in a rat model of stress urinary incontinence. Nanomedicine Nanotechnol Biol Med. 2020 Nov;30:102281.
53. Wang K, Liu T, Zhang Y, Lv H, Yao H, Zhao Y, et al. Combined Placental Mesenchymal Stem Cells with Guided Nanoparticles Effective Against Diabetic Nephropathy in Mouse Model. Int J Nanomedicine. 2024;19:901–15.
54. Li X, Wei Z, Zhang W, Lv H, Li J, Wu L, et al. Anti-Inflammatory Effects of Magnetically Targeted Mesenchymal Stem Cells on Laser-Induced Skin Injuries in Rats. Int J Nanomedicine. 2020 Aug;Volume 15:5645–59.
55. Li X, Wei Z, Wu L, Lv H, Zhang Y, Li J, et al. Efficacy of Fe3O4@polydopamine nanoparticle-labeled human umbilical cord Wharton's jelly-derived mesenchymal stem cells in the treatment of streptozotocin-induced diabetes in rats. Biomater Sci. 2020 Oct 7;8(19):5362–75.
56. Wang X, Bai R. Advances in smart delivery of magnetic field-targeted drugs in cardiovascular diseases. Drug Deliv. 2023 Dec;30(1):2256495.
57. Molaei MJ. Magnetic hyperthermia in cancer therapy, mechanisms, and recent advances: A review. J Biomater Appl. 2024 Jul;39(1):3–23.
58. Cheng HLM. A primer on in vivo cell tracking using MRI. Front Med. 2023;10:1193459.
59. Wang W, Shang S, Wang Y, Xu B. Utilization of nanomaterials in MRI contrast agents and their role in therapy guided by imaging. Front Bioeng Biotechnol. 2024;12:1484577.
60. Pipatwatcharadate C, Iyer PR, Pissuwan D. Recent Update Roles of Magnetic Nanoparticles in Circulating Tumor Cell (CTC)/Non-CTC Separation. Pharmaceutics. 2023 Oct 17;15(10):2482.
61. Byun H, Lee S, Jang GN, Lee H, Park S, Shin H. Magnetism-controlled assembly of composite stem cell spheroids for the biofabrication of contraction-modulatory 3D tissue. Biofabrication. 2021 Nov 11;14(1).
62. Hu H, Krishaa L, Fong ELS. Magnetic force-based cell manipulation for in vitro tissue engineering. APL Bioeng. 2023 Sep;7(3):031504.
63. Mocanu-Dobranici AE, Costache M, Dinescu S. Insights into the Molecular Mechanisms Regulating Cell Behavior in Response to Magnetic Materials and Magnetic Stimulation in Stem Cell (Neurogenic) Differentiation. Int J Mol Sci. 2023 Jan 19;24(3):2028.
64. Xu R, Xu Q. A Survey of Recent Developments in Magnetic Microrobots for Micro-/Nano-Manipulation. Micromachines. 2024 Mar 29;15(4):468.
65. Xu Z, Neuber S, Nazari-Shafti T, Liu Z, Dong F, Stamm C. Impact of procedural variability and study design quality on the efficacy of cell-based therapies for heart failure - a meta-analysis. PloS One. 2022;17(1):e0261462.
66. Hinkle JW, Mahmoudzadeh R, Kuriyan AE. Cell-based therapies for retinal diseases: a review of clinical trials and direct to consumer 'cell therapy' clinics. Stem Cell Res Ther. 2021 Oct 11;12(1):538.
67. Fernández-Garza LE, Barrera-Barrera SA, Barrera-Saldaña HA. Mesenchymal Stem Cell Therapies Approved by Regulatory Agencies around the World. Pharm Basel Switz. 2023 Sep 21;16(9):1334.
68. Kamei N, Ochi M, Adachi N, Ishikawa M, Yanada S, Levin LS, et al.

[Downloaded from mjiri.iums.ac.ir on 2026-10-14]

[DOI: 10.47176/mjiri.39.91]

The safety and efficacy of magnetic targeting using autologous mesenchymal stem cells for cartilage repair. Knee Surg Sports Traumatol Arthrosc Off J ESSKA. 2018 Dec;26(12):3626–35.
69. Miceli V, Bulati M, Iannolo G, Zito G, Gallo A, Conaldi PG. Therapeutic Properties of Mesenchymal Stromal/Stem Cells: The Need of Cell Priming for Cell-Free Therapies in Regenerative Medicine. Int J Mol Sci. 2021 Jan 14;22(2):763.
70. Chen DX, Lu CH, Na N, Yin RX, Huang F. Endothelial progenitor cell-derived extracellular vesicles: the world of potential prospects for the treatment of cardiovascular diseases. Cell Biosci. 2024 Jun 5;14(1):72.
71. Li J, Ma Y, Miao XH, Guo JD, Li DW. Neovascularization and tissue regeneration by endothelial progenitor cells in ischemic stroke. Neurol Sci Off J Ital Neurol Soc Ital Soc Clin Neurophysiol. 2021 Sep;42(9):3585–93.
72. Garg P, Pareek S, Kulkarni P, Horne D, Salgia R, Singhal SS. Next-Generation Immunotherapy: Advancing Clinical Applications in Cancer Treatment. J Clin Med. 2024 Oct 30;13(21):6537.
73. Gandarias L, Gubieda AG, Gorni G, Mathon O, Olivi L, Abad-Díaz-de-Cerio A, et al. Intracellular transformation and disposal mechanisms of magnetosomes in macrophages and cancer cells. Biotechnol J. 2023 Oct;18(10):e2300173.
74. Zhao F, Zhao Y, Liu Y, Chang X, Chen C, Zhao Y. Cellular uptake, intracellular trafficking, and cytotoxicity of nanomaterials. Small Weinh Bergstr Ger. 2011 May 23;7(10):1322–37.
75. Brubaker DK, Lauffenburger DA. Translating preclinical models to humans. Science. 2020 Feb 14;367(6479):742–3.
76. Lal S, Li A, Dos Remedios C. Limitations in Translating Animal Studies to Humans in Cardiovascular Disease. J Cardiovasc Transl Res. 2016 Apr;9(2):165–6.
77. Shi CL, Zhang YS, Jiao HG. Numerical Study on Magnetic Field Characteristics of Typical Permanent Magnet. Mater Sci Forum. 2012;704–705:1073–8.
78. Turchyn VV, Legenkiy YuA, Solopov MV, Popandopulo AG, Bespalova SV, Fistal EYa. Magnetophoretic properties of human fetal fibroblasts magnetically labeled with citrate stabilized superparamagnetic iron oxide nanoparticles (In Russian). Genes Cells. 2017;12(1):47–53.
79. Loewe A, Martínez Díaz P, Nagel C, Sánchez J. Cardiac Digital Twin Modeling. In: Jadczyk T, Caluori G, Loewe A, Golba KS, editors. Innovative Treatment Strategies for Clinical Electrophysiology [Internet]. Singapore: Springer Nature; 2022 [cited 2025 Jun 5]. p. 111–34. Available from: https://doi.org/10.1007/978-981-19-6649-1_7
80. Mone G. Biomedical Digital Twins. Commun ACM. 2023 Sep 22;66(10):9–11.
81. Benson M, Loscalzo J, Mahmud AF, Aly DMA, Rzhetsky A, Zitnik M, et al. Digital Twins as Global Learning Health and Disease Models of Individuals [Internet]. Preprints; 2024 [cited 2025 Jun 5]. Available from: https://www.preprints.org/manuscript/202406.0357/v1

[Downloaded from mjiri.iums.ac.ir on 2026-10-14]

[DOI: 10.47176/mjiri.39.91]

Appendix Table A1. Experimental parameters and outcomes of magnetic cell targeting in in vivo models (detailed)

Experimental design			Magnetic trap		Effects of magnetic targeting relative to control	Ref.
Animal model	Cells, magnetic tag	Route of administration, cell dose	Type, dimensions, induction (B), location	Exposure time		
Nervous system disease models						
Wistar rats, a model of traumatic sciatic nerve injury.	MMSCs from rat AT, SPION-Cit	IV, 6-7x10^6/300 µl saline solution	NdFeB (13x23x1 mm), 0,16 T, the area of sciatic nerve damage.	24 hours	After 6 days: ↑ homing ×2.16, ↑ myelinated axons ×3.8, ↑ myelin protein ×1.8, ↓ distal latency ×2.12	(46)
Newborn Sprague-Dawley rats, hypoxic-ischemic brain injury (ligation of the left common carotid artery).	MMSCs from rat BM, SPION-PLL	ICV, 10^5/5 µl	NdFeB, 0,39 T, left side of the head.	2 hours	After 4 weeks: ↑ diffusion coefficient +65%, ↑ diffusion fraction +33%, ↓ apoptosis ~60×.	(48)
C57BL6/J neonatal P0-7 mice, a model of cerebral arterial thrombosis by magnetic erythrocytes.	Mouse erythrocytes, SPION-biotin-streptavidin-SiO_2	IV (superficial temporal vein), equivalent to 6 mg Fe/kg.	NdFeB, cylinder (1*1 mm), 0.25-0.5 pN, occipital and neck region, on the skull in the area of the distal middle cerebral artery (dMCA).	10 hours	After 30 min 50% hypoperfusion of dMCA (plateau). After 6 h - massive neurodegeneration. After 7 h of occlusion - infarction of 15% of brain volume.	(47)
Sprague-Dawley rats, hypoxic-ischemic brain injury (ligation of the left common carotid artery).	MMSCs from rat BM, SPION-PLL	ICV, 10^5/5 µl	NdFeB, 0,118 T, left side of the occipital protrusion.	2 hours	After 4 weeks: ↓ mean kurtosis ×2 (MRI data), ↓ edema, ↓ microglia infiltration, ↓ apoptosis.	(17)
Sprague-Dawley rat, males, a model of intracerebral hemorrhage.	Spherical neuronal masses from human ESCs, FION	IV, 4*10^6/500 µl PBS	Two rectangular NdFeB magnets (5x10x2 мм) built into the helmet, 0,32 T, left anterior skull.	3 days	After 3 days: ↑ cell concentration at injury site ×2.1, ↓ brain edema, ↓ IL-1β ×2, ↓ pERK −17%, ↓ COX-2 ×2.8. 42 days: ↓ brain atrophy −36%.	(19)
C57/BL6 mice, male, cerebral infarction model (permanent middle cerebral artery occlusion).	Human MMSCs from the UC, SPION-PDA	IV (tail vein), 5x10^5 in PBS (24 h after surgery)	Permanent magnet, fixation on the head.	5 days	↓ infarct area −41%, ↓ M1 microglia polarization, ↑ M2 microglia infiltration, ↑ MAP2 +26%, ↑ NeuN +30% in infarct zone.	(49)
Sprague-Dawley rats, males, carotid artery injury (left common carotid artery clamping and reperfusion with balloon catheter).	MMSCs from rat BM, lipid-polymer nanocapsules - SPION-PLGA-PEG	Intra-arterially (left common carotid artery), 5x10^6/20 µl PBS	Two permanent cubic magnets (4 mm), 0,3 T, in the area under the left common carotid artery.	5 minutes	↑ cell retention at injury site ×20 (immediately), ×5 (after 24 h).	(25)
Albino rats, males, a model of facial nerve palsy.	MMSCs from rat BM, SPION-PLL	IV (tail vein), 10^6/0,2 ml DMEM/F12	NdFeB, disc (5x2 mm), 0,57 T, from below the right ear.	24 hours	Magnetic labelling of MMSCs had a negative effect on the processes of facial nerve regeneration.	(28)
Mice transgenic APP/PS1 lines, a model of Alzheimer's disease.	MMSCs from human UC blood, SPION-PDA	IV (tail vein), 2x10^5/100 µl	NdFeB, cylinder (diam. 20 mm), in front of the head.	12 hours	After 10 days: ↑ MMSCs in hippocampus, improved memory (↓ escape latency in water maze −43%).	(50)
Wistar rats, male, Alzheimer's disease model (8 µg/kg amyloid β 1-42).	MMSCs from human WJ, SPION-dextran	ICV, IV, 10^6/animal	Halbach array (12 cubic 1 cm NdFeB magnets, inner diam. 3 cm, outer diam. 8 cm), 0.2 T, around the head.	2 hours	After IV administration: 8 weeks: ↑ MSCs in hippocampus +16%, ↑ memory & cognition +24-58%; 10 weeks: ↑ ChAT +28%, ↑ AChE +20%, ↓ apoptosis −59%.	(39)
5xFAD mice, a model of Alzheimer's disease.	MMSCs from human WJ, SPION (Ferumoxytol)	ICV (right lateral ventricle), 10^5/7 µl.	Permanent magnet, cranial fixation.	3 days	↑ MMSCs retention in brain ×7. After 7 days: ↓ β-amyloid −44%. After 3 weeks (3 doses): ↑ cognitive functions +24-60%.	(22)
Rat model of Parkinson's disease (injection of 6-hydroxydophamine into the right medial forebrain bundle).	MMSCs from rat AT, SPION-PLL	locally into the right medial bundle of the forebrain, 3x10^5/9 µl of saline solution	NdFeB, 0,32 T, on the skull in the area of the right medial bundle of the forebrain.	1 week	↑ cell retention +77%. After 3 weeks: ↓ apomorphine-induced rotation −15%. After 6 weeks: ↓ apomorphine-induced rotation −22%.	(51)

[Downloaded from mjiri.iums.ac.ir on 2026-10-14]

[DOI: 10.47176/mjiri.39.91]

Appendix Table A1. Experimental parameters and outcomes of magnetic cell targeting in in vivo models (detailed)

Experimental design			Magnetic trap		Effects of magnetic targeting relative to control	Ref.
Animal model	Cells, magnetic tag	Route of administration, cell dose	Type, dimensions, induction (B), location	Exposure time		
Nervous system disease models						
Wistar rats, a model of Parkinson's disease (injection of 6-hydroxydophamine into the right striatum).	MMSCs from human nasal mucosa, SPION-alginate	intranasal drip, 8 ml of suspension in conditioned medium into each nostril	Halbach array (12 cubic 1 cm NdFeB magnets, inner diam. 3 cm, outer diam. 8 cm), 0.2 T, around the head.	8 weeks	Week 4: ↑ motor functions +85% (rotarod), +53% (open field). Week 8: ↑ dopamine neurons in substantia nigra +63%, ↑ Nurr1 +32%, ↑ DAT +11%, ↑ Pitx3 +42%.	(40)
Bald athymic BALB/c mice	MMSCs from the human nasal turbinate, SPION-PLL	intranasally (through the lattice bone into the olfactory bulb), 10^6/10 µl PBS	Permanent cylinder magnet, 0.02 T, occipital and neck area.	2 days	Introduced MMSCs were found in the frontal cortex only in the magnetic field group.	(38)
Models of diseases of the urinary system						
Rabbits, white Japanese, resection of the anterior bladder wall by transuterine electrofulguration.	MMSCs from rabbit BM, SPION ferucarbotran	bladder cavity, 10^6/animal	NdFeB (130x130x47 mm), 1 T, externally in the resection area.	10 minutes	After 14 days: ↑ repair area ×2. MMSCs groups: ↑ vascularization and myofibrosis volume ×2.3.	(45)
Sprague-Dawley rats, female, stress urinary incontinence model (vaginal balloon dilatation and bilateral ovarian excision).	Myoblasts from rat AT MMSCs, SPION- PVP-PLL	transuterally (to the urethral sphincter area), 1,5x10^6/200 µl PBS	NdFeB, toroidal (outer diam. 8 mm, inner diam. 4 mm), 0,19 T, externally around the injection site.	20 minutes	After 14 days: ↑ cell retention at injection site, ↑ urethral sphincter thickness. MMSCs groups: leak point pressure ~ sham-operated control.	(52)
C57BL/6J mice, diabetic nephropathy model (streptozotocin 30 mg/kg, high-fat diet).	MMSCs from human placenta, SPION-PDA	IV (tail vein), 5x10^5/200 µl PBS	Permanent magnet, 1.2 T, externally in the kidney area.	20 minutes	After 28 days: ↑ cell retention in kidney; ↓ serum urea nitrogen −17% and creatinine −34%; ↓ urinary creatinine −29%, albumin −24%; ↓ renal IL-2 −34%, IL-6 −23%, IFN-γ −21%, TNF-α −40%; ↓ plasma TGF-β −11%. MMSCs groups: ↓ nephropathy signs, ↓ cytokines, ↓ water intake ~2×, ↑ body weight +20%, ↓ kidney weight −13%, renal index −25%.	(53)
Sprague Dawley rats, male, renal ischaemia-reperfusion (right nephrectomy, left renal artery clamp 40 min).	EPCs from rat AT, SPION-PEG-anti-CD-133	IV (tail vein), 2x10^6/200 µl PBS	Permanent magnet, externally in the area of the left kidney.	30 minutes	3 days: ↑ homing ×2.15; ↓ serum urea nitrogen ×2.46, creatinine ×2.06; ↓ apoptosis ×2.65; ↑ renal parenchyma proliferation ×3.48.	(33)
Models of eye disease						
MYOC-Y437H transgenic mice, a model of glaucoma.	TMCs from iPSCs, SPION- PLGA-Cypate	anterior chamber of the eye, 75x10^3/3 µl	Ring magnet, 0,03-0,06 T, iridocorneal angle	15-45 minutes	60 mT, 15 min: ↑ TMCs retention in trabecular meshwork ×2.8-3.9 (28.7% total), uniform distribution; temporary ↓ IOP for 10 days (−8.8% on day 8).	(12)
MYOC-Y437H transgenic mice, a model of glaucoma.	MMSCs from human AT, TMCs from iPSCs, SPION-amine	anterior chamber of the eye, 1,5x10^3/1,5 µl	Point magnet (NdFeB N52 + thin stainless-steel cylinder), 0,25 T, iridocorneal angle	No data	↓ IOP: −27% (9 months, MMSCs), −13% (3-4 months, TMCs).	(11)
NZW rabbits, a model of corneal endothelial dysfunction (partial removal of descemet membrane or endothelial layer).	Human corneal endothelial cells (GFP^+), SPION-SiO_2	anterior chamber of the eye, 2-6x10^5/100-250 µl Hanks' solution	NdFeB, cylinder (12x20 mm), outer side of the closed eyelid in the corneal area.	3 hours	After 7 days: ↓ corneal edema −37%. After 14 days: slight ↑ corneal transparency.	(42)
Chinchilla rabbits	MMSCs from mouse BM (culture conditions: 5% O_2 and 21% O_2), Dynabeads M-280-Pluronic L-123	Subretinally, 10^4/50 µl of growth medium	Polymer disc magnetic implant, 7x0.35 mm, 0.005 T, upper outer quadrant of the eyeball.	15 days	MMSC retention under retina: Day 6: MMSC-5%O_2 > MMSC-21%O_2. Day 9: Few MMSC-5%O_2, no MMSC-21%O_2. Day 12: No MMSCs in all groups.	(43)

[Downloaded from mjiri.iums.ac.ir on 2026-10-14]

[DOI: 10.47176/mjiri.39.91]

Appendix Table A1. Experimental parameters and outcomes of magnetic cell targeting in in vivo models (detailed)

Experimental design			Magnetic trap		Effects of magnetic targeting relative to control	Ref.
Animal model	Cells, magnetic tag	Route of administration, cell dose	Type, dimensions, induction (B), location	Exposure time		
Models of ischemic heart disease						
C57B6 mice, an ischemia-reperfusion model.	Human MMSCs, SPION-SiO_2-IGF	intramyocardial, 10^5 in 20 µl of DMEM/Matrigel 1:1	Permanent magnet, in the area of the left ventricle closer to the apex of the heart.	7 days	↑ mean LVEF: +11% (day 30), +21% (day 60); ↓ cardiomegaly −43% and fibrosis level.	(18)
Lewis rats, male, myocardial infarction model (ligation of the left anterior descending artery).	Rat endothelial cells, FluidMAG D	epicardially as part of a magnetic device, cell dose – no data.	Bilayer epicardial implant (PGS-PCL/PGS-NdFeB), the epicardial surface of the infarcted area.	28 days	Day 14: angiogenesis with host vessel integration in magnetic device zone; ↑ implantation area ×4.6, perfusion ×3.14. Day 28: ↑ LVEF +10%, ↓ infarct area −38%, fibrosis −50%; ↑ wall thickness +30%, perfusion in implant zone +32%.	(15)
Sprague-Dawley rats, female, myocardial infarction, (ligation of the left anterior descending artery, formation 7 days).	EPCs from rat BM, SPION-SiO_2	IV (tail vein), 10^6/100 µl PBS	Permanent cylindrical magnet, 0.39 T, infarct area.	1 hour	After 4 weeks: ↑ cell retention in infarct zone ×3, ↑ LVEF +11%, ↓ infarct area −35%, myocardial apoptosis −29%; ↓ Col-I −28%, Col-III −41%, TGF-β −24%. ↑ microvessel density and angiogenesis factors: VEGF +48%, IGF-1 +31%, PDGF +27%, SDF-1α +28%, β-FGF +32%.	(14)
Models of cancer disease						
C57BL/6 mice, female, grafted tumor line EG7-OVA (lymphoma).	Mouse CTLs (OT-I), SPION-APS	IV, 8x10^6/100 µl PBS	NdFeB, disc (8x6 mm), 1.45 T, near the tumor.	90 minutes	After 14 days: ↓ tumor infiltration −21%, ↑ tumor volume ×2.03, ↑ CTLs in tumor-draining lymph nodes ×2.17.	(35)
C57BL/6 and BALB/c mice inoculated with tumor lines EG7 (lymphoma) and 4T1 (breast cancer).	Mouse CTLs and TILs, SPION-PEG-anti-PD-1 polyclusters	IV, 0,5-1x10^7/animal	NdFeB, outside the tumor area.	12 hours	↑ CTLs and TILs tumor infiltration ×3. Complete tumor suppression and 100% survival for 35 days in magnet groups.	(24)
CBA mice, grafted tumor line Sa-37 (sarcoma, left femur).	Mouse DCs, SPION-Sa-37 antigens	intradermally, 3 times, 10^6/animal	NdFeB, 20 pN, inguinal lymph nodes.	1 hour	After 28 days: ↓ tumor volume −45% and tumor weight −31%; ↓ TGF-β ×3.5, ↑ IL-10 ×5, VEGF ×3 (in tumor); ↑ IL-4 ×2, IFN-γ ×4.5 (in lymph nodes).	(44)
BALB/c mice, grafted tumor line G422 (brain glioma).	Neutrophils, SPION-gelatin-paclitaxel-E. coli membrane	IV (tail vein), 3x10^6/animal	RMF device (5 mT, 1 Hz), glioma area.	1 hour	After 3 hours: ↑ homing with RMF ×2.7; ↑ mean survival time: +17% (RMF only), +30% (with chemoattraction).	(29)
Models of musculoskeletal diseases						
C57BL/6J mice, female, muscle inflammation model (20 µl of 0.5% bupivacaine into the left tibialis anterior muscle).	Mouse MMSCs, anionic SPION liposomes	intramuscularly (tibialis anterior muscle), 5x10^5/animal	Permanent magnet, left tibialis anterior muscle area.	3 hours	After 6 h: ↑ cell retention in muscle ×2. After 24 h: cells detected only in magnet group. After 5 days: ↓ TNF-α ×1.9 and IL-1β ×3.1; ↑ IL-6 ×2.3 and IL-10 ×1.5. After 7 days: ↓ signal ×10.	(20)
NZW rabbits, osteoarthritis model (anterior cruciate ligament dissection, formation 6 weeks).	NZW rabbit chondrocytes,SPION-gelatin	Joint capsule, cell dose – no data.	Permanent magnet, cylinder (1x3 mm), implantation in the medial femoral condyle.	8 weeks	After 8 weeks: ↑ proteoglycan secretion in joint +51%.	(16)

[Downloaded from mjiri.iums.ac.ir on 2026-10-14]

[DOI: 10.47176/mjiri.39.91]

Appendix Table A1. Experimental parameters and outcomes of magnetic cell targeting in in vivo models (detailed)

Experimental design			Magnetic trap		Effects of magnetic targeting relative to control	Ref.
Animal model	Cells, magnetic tag	Route of administration, cell dose	Type, dimensions, induction (B), location	Exposure time		
Other animal models						
C57BL/6 mice, pulmonary silicosis (SiO_2 20 mg/50 µl saline solution intratracheally).	Mouse MMSCs from BM, SPION-Cit	IV (internal jugular vein), $3x10^5$/50 µl saline	Two disc NdFeB magnets (12x4 mm, N42), in the chest area.	48 hours	↑ homing ×3.8. ↓ lung static elastance −29%, resistive pressure −60%, granuloma area −36%, IL-1β −50%.	(34)
C57BL/6 mice, ototoxicity model (kanamycin and furosemide injection).	Mouse MMSCs, SPION-PLGA	IV, intratympanal, cell dose – no data	NdFeB, cubic (5 mm), skull apex, subcutaneously	24 hours	Magnetic delivery of MMSCs to the cochlear apparatus is 1.92 times higher with intravenous administration.	(13)
Rat, a model of full-thickness skin burns.	Rat MMSCs from BM, SPION-SDS	IV (tail vein), 10^6/1 ml PBS	NdFeB, 1,2 T, under the wound.	30 minutes	After 7 days: MMSCs accumulation detected only in magnet group; ↑ serum VEGF +21%, ↓ IL-6, IL-1α, IL-2 −25%. Local anti-inflammatory effect in all MMSCs groups.	(54)
C57BL/6 mice and bald athymic mice.	Human (Jurkat) and mouse T-cells, SPION-APS	IV, 10^7/100 µl	NdFeB, disc-shaped (8x6 mm), 1.45 T, in the popliteal lymph node area.	30-90 minutes	↑ homing to popliteal lymph nodes ×2.4-2.9.	(36)
Rats, a model of streptozotocin induced diabetes.	Rat MMSCs from WJ, SPION-PDA	IV (tail vein), 10^6/1 ml PBS	NdFeB, 1.2 T, dorsally in the pancreatic gland area	30 minutes	2 weeks: ↑ cell retention +38%. 3 weeks: ↑ β-cell proportion in gland and C-peptide in serum +48%, ↓ β-cell apoptosis −34%.	(55)
BALB/c and C57 mice, females.	Mouse erythrocytes, SPION-DMSA	IV (tail vein), $315x10^6$ in 300 µl	Electromagnet, 0.8 T, magnetic field focus in the tail, back, limbs and brain area.	30 minutes	Intravascular formation of spherical aggregates of erythrocytes stable for 6 h at the focus of the magnetic field. Capture efficiency 80% inside the vessel at a distance of 1 mm (in silico data).	(41)
Wistar rats, subcutaneous cell retention using a magnetic field.	Human MMSCs, MPIO-SiO_2 (SiMAG)	Subcutaneously A) abdominally, B) knee joint area; 10^6/100 µl	A) NdFeB, cylinder (3x12 mm), 0.3 T, subcutaneously, abdominally. B) NdFeB, disc (12x4 mm), 0.325 T, externally in the knee joint area.	A) 20 min. B) time of 20 full flexions of the hind limb.	A) More pronounced cell retention with magnet. B) ↑ MMSCs retention ×2 after first bending series, ×3.5 after second.	(37)
ICR mice, females.	Macrophage-like cell line RAW264, cationic SPION-liposomes	intradermally, 10^6/animal	Permanent magnet, abdominal area.	1 hour	↑ cell retention in rectum ×2.4 after 6 h, ×9.1 after 24 h.	(23)

Abbreviations: AChE – acetylcholinesterase; APS – 3-aminopropyltriethoxysilane; AT – adipose tissue; BM – bone marrow; ChAT – choline acetyltransferase; Cit – citrate; Col. I-III – collagen type I-III; COX-2 – cyclooxygenase-2; CTLs – cytotoxic T lymphocytes; DAT – dopamine transporter; DMSA – dimercaptosuccinic acid; EPCs – endothelial progenitor cells; ESCs – embryonic stem cells; FION – ferrimagnetic iron oxide nanocubes; GFP – green fluorescent protein; ICV – intracerebroventricular; IFN-γ – interferon gamma; IGF – insulin-like growth factor; IL – interleukin; IV – intravenous; β-FGF – basic fibroblast growth factor (FGF-2); LVEF – left ventricular ejection fraction; MAP2 – microtubule-associated protein 2; MPIO – microparticles of iron oxide; MRI – magnetic resonance imaging; MMSCs – multipotent mesenchymal stromal cells; NdFeB – neodymium-iron-boron; NeuN – neuronal nuclear antigen; Nurr1 – nuclear receptor related 1 protein; PBS – phosphate-buffered saline; PCL – polycaprolactone; PDA – polydopamine; PDGF – platelet-derived growth factor; PEG – polyethylene glycol; pERK – phosphorylated extracellular signal-regulated kinase; PGS – polyglycerol sebacate; Pitx3 – paired-like homeodomain transcription factor 3; PLGA – poly(lactic-co-glycolic acid); PLL – poly-L-lysine; pN – piconewton; PVP – polyvinylpyrrolidone; RMF – rotating magnetic field; SDF-1α – stromal cell-derived factor 1 alpha; SPION – superparamagnetic iron oxide nanoparticles; T – Tesla (the unit of magnetic flux density); TGF-β – transforming growth factor beta; TILs – tumor-infiltrating lymphocytes; TMCs – trabecular meshwork cells; TNF-α – tumor necrosis factor alpha; UC – umbilical cord; VEGF – vascular endothelial growth factor; WJ – Wharton's jelly.

[Downloaded from mjiri.iums.ac.ir on 2026-10-14]

[DOI: 10.47176/mjiri.39.91]

Magnetic Cell Targeting

Appendix Table A2. Experimental parameters and outcomes of magnetic cell targeting in in vitro models

Cells, magnetic tag	Experiment	Magnetic trap, induction (B), exposition time	Main results	Ref.
Mouse MMSCs, SPION-PLGA polyclusters	A) Cell migration to MF in Transwell chamber with chemoattraction (SDF-1). B) Migration into MF in a culture vessel.	A) NdFeB cubic (5 mm), B=n/d, Exp.: 24 h. B) NdFeB cubic (3 mm), B=0.34 T, Exp.: 24 h and 48 h.	A) ↑ migration ×2 with MF. B) Cell distribution from MF source: 0-5 mm – 50%, 5-10 mm – 30%, 10-15 mm – 10%.	(13)
Human (Jurkat) and mouse T-cells, SPION-APS	A) Cell migration in MF in Transwell chamber with chemoattraction (CXCL12 or CCL21). B) Cell capture in flow in MF in a channel slide (μ-Slide I Luer, 50x5x0.4 mm, flow rate 100 μl/min).	A) NdFeB (8x6 mm), B=1.45 T. Exp.: 16 h. B) A system of two NdFeB magnets (5x14 mm, B=1.35 T and 8x6 mm, B=1.45 T) placed at opposite poles. Exp.: 2 min.	A) ↑ migration in MF with chemoattraction +10%. B) Magnetic capture in flow more effective for Jurkat T-cells; minimum magnetic susceptibility threshold: 5 pg Fe/cell.	(36)
Mouse CTLs (OT-I), SPION-APS	A) Cell migration in MF in Transwell chamber with chemoattraction (CXCL12). B) Cell capture in flow in MF in a channel slide (μ-Slide I Luer, 50x5x0.4 mm, flow rate 100 μl/min).	A) NdFeB (8*6 mm), B=1.45 T. Exp.: 16 h. B) A system of two NdFeB magnets (5x14 mm, B=1.35 T and 8x6 mm, B=1.45 T) placed at opposite poles. Exp.: 2 min.	A) ↑ migration in MF with chemoattraction +11.4%. B) Magnetic capture at 150 μgFe/mL > 100 μgFe/mL by ×2.46.	(35)
TMCs from iPSCs, SPION- PLGA-Cypate	A) Magnetic capture of cells in a 15-ml tube. B) Magnetic capture of cells on the side of the culture vessel. C) Magnetic capture in vertical flow (flow rate 0.8 ml/min).	A) Cylindrical permanent magnet, B=0.389 T. Exp.: n/d. B, C) Rectangular permanent magnet, B=0.143 T. Exp.: B) 8 h, C) n/d.	A) Cell concentration in the MF zone. B) Capture and adhesion: 20.7% of cells on the vessel's lateral surface. C) Magnetic capture distance: 30 mm; average magnetophoresis speed: 0.66 μm/s.	(12)
Human MMSCs, SPION-SiO_2-IGF	A) Magnetic cell capture in a T25 vertical vial. B) Magnetic cell capture in flow (diam.=0.86 mm, velocity 2.8-14.6 ml/min, shear stresses 7-35 dyne/cm^2).	A) Permanent magnet, B= n/d. Exp.: 2 d. B) Permanent magnet, B= n/d. Exp.: n/d.	A) Cell density in the MF zone: 5850/cm² (0 without MF). B) Retention: 85% of cells at shear stress 12.8 dyne/cm² (typical for the human left ventricle), >58% at 27 dyne/cm².	(18)
Human MMSCs, MPIO-SiO_2 (SiMAG)	A) Magnetic capture of cells under orbital agitation. B) Magnetic capture of cells in flow (diam. 2 mm, velocity 333 μl/min, shear stress 5.09 dyne/cm^2). C) Vertical migration in MF in hydrogel. D) Horizontal migration into MF in hydrogel. E) Migration into MF in a porous scaffold. F) Magnetic trapping of cells in a suspended drop model. G) Migration of adherent cells in MF. H) Two-dimensional migration of cells in MF.	A and B) System of two disc NdFeB magnets (8x4 mm, B=0.36 T and 12x4 mm, B=0.325 T). Exp: A) 24 h and 48 h, B) 30 min. C) Magnetic separator for 24-well plates, B= n/d. Exp: 72 h. D) NdFeB disc (10x5 mm, B= n/d). Exp: 5 d. E) NdFeB disc. Exp.: 72 h. F, H) NdFeB disc (10x3 mm, B=0.28 T). Exp: F) 24 h, H) 8 h. G) Two NdFeB discs (5x4 mm, B=0.4 T). Exp: 48 h.	A) Cell concentration highest in the zone of maximum MF gradient. B) Magnet 8x4 mm: 45% cell capture; 12x4 mm: 90% cell capture. C) ↑ vertical migration ×1.85 in magnetic field (with 20 μg Fe/mL labeling). D) ↑ horizontal migration +13% in MF; 1% of cells reached the bottom (50% in control). E) Deeper penetration of labeled cells into the scaffold. F) Cell capture and adhesion counteracting gravity in MF. G) Migration and accumulation of adhered cells in the MF zone. H) Cell migration toward magnet +63% vs. control.	(37)

[Downloaded from mjiri.iums.ac.ir on 2026-10-14]

[DOI: 10.47176/mjiri.39.91]

Appendix Table A2. Experimental parameters and outcomes of magnetic cell targeting in in vitro models

Cells, magnetic tag	Experiment	Magnetic trap, induction (B), exposition time	Main results	Ref.
MMSCs from the human nasal turbinate, SPION-PLL	Magnetic targeting in a microfluidic channel.	A) RMF device (Nano-Mag, Aeon Scientific, B=22 mT, frequency 3 Hz). B) permanent cylindrical magnet (7x30 mm, B=20 mT). Exp.: 24 h.	Magnetically controlled cell movement with overcoming mechanical obstacles is demonstrated.	(38)
Mouse erythrocytes, SPION-biotin-streptavidin-SiO_2	Concentration of red blood cells in a droplet in MF.	Rectangular permanent magnet (50x20x5 mm, B=n/d). The edge of the magnet is set in the middle of the suspension drop.	Line up magnetic red blood cells in a row parallel to the edge of the magnet for 90 s.	(47)
MMSCs from human WJ, SPION (Ferumoxytol)	A) Magnetic capture of cells in a 15-ml tube. B) Magnetic capture of cells in flow conditions.	A) Permanent magnet, B=n/d, Exp.: n/d. B) Permanent magnet, B=n/d, Exp: 10 min.	A) Cell concentration in the MF zone. B) Capture efficiency of 25-35%.	(22)
Mouse DCs, SPION-Sa-37 antigens	Migration of adherent cells in Petri dishes in MF.	NdFeB disc, B= 0.084 T, Exp: n/d.	Migration of cells towards the magnet.	(44)
Macrophage-like cell line RAW264, cationic SPION-liposomes	Adhesion of RAW264 cells to a monolayer of the Caco-2 cell line in MF.	Permanent magnet (8x12x1 cm), B=0.3 T, Exp.: 5 min.	↑ adhesion of RAW264 to Caco-2 monolayer in magnetic field compared to control.	(23)
Mouse MMSCs, anionic SPION liposomes	Magnetic cell capture in a cell culture plate.	Permanent magnet (B=n/d). Exp.: 10 min.	Concentration of cells in the MF area.	(20)
Rat endothelial cells, FluidMAG D	A) Capture magnetic cells in suspension ($2.5x10^6$/ml in PBS) and incubation on a magnetic device. B) Migration of cells into MF in Transwell chamber.	A) Magnetic device: bilayer epicardial implant (protective layer - PGS-PCL, magnetic layer - PGS-NdFeB). B=0.058 T on the surface of the magnetic layer. Exp: 5 d. B) Fragment of the magnetic device A). Exp.: 12 h.	A) Uniform accumulation of magnetic cells on implant (>2×10⁴/cross-field); formation of vessel-like structures by day 5. B) ↑ cell migration in magnetic field ×2.6.	(15)
MMSCs from rabbit BM, SPION ferucarbotran	Magnetic cell capture in a cell culture flask.	NdFeB (130x130x47 mm, B=1 T), flask side wall. Exp: n/d.	Concentration of cells near the lateral wall in the MF area.	(45)
Mouse MMSCs from BM, SPION-Cit	A) Magnetic capture of cells in a cell culture plate. B) Cell migration in MF in Transwell chamber with chemoattraction (SiO_2 activated macrophages).	System of two disc NdFeB magnets (12x4 mm, N42, B=n/d). Exp.: A) 24 h, B) 15 h.	A) Cell concentration in the MF zone. B) ↑ cell migration in MF +50%; ↑ CCR2 expression ×4.6, CXCR4 ×3.5.	(34)
Myoblasts from rat AT MMSCs, SPION- PVP-PLL	Magnetic capture of cells in Petri dishes.	NdFeB toroidal (external diam. 8 mm, internal diam. 4 mm, B=0.19 T). Exp.: 24 h.	Concentration of cells along the toroid ring.	(52)
EPCs from rat AT, SPION-PEG-anti-CD-133	Cell migration in MF in a Transwell chamber.	Permanent magnet (B=n/d). Exp.: 24 h.	↑ cell migration in MF ×2.	(5)
NZW rabbit chondrocytes, SPION-gelatin	Magnetic capture of cells in Petri dishes.	NdFeB (N52, B=0.4 T). Exp.: 7 d.	Monolayer cell aggregation under MF. ↑ proteoglycan secretion +28% at 7 days. ↑ chondrogenesis gene expression (collagen II, SOX9, TIMP3, Aggrecan). ↓ collagen I and MMP13.	(16)

[Downloaded from mjiri.iums.ac.ir on 2026-10-14]

[DOI: 10.47176/mjiri.39.91]

Magnetic Cell Targeting

Appendix Table A2. Experimental parameters and outcomes of magnetic cell targeting in in vitro models

Cells, magnetic tag	Experiment	Magnetic trap, induction (B), exposition time	Main results	Ref.
EPCs from rat BM, SPION-SiO_2	A) Magnetic capture of cells in a Petri dish. B) Cell capture in a 15 ml centrifuge tube in an oscillating shaker (simulation of flow conditions).	NdFeB cylinder (B=0.39 T). Exp.: A) 24 h, B) 15 min.	Concentration of cells in the area of MF action.	(14)
MMSCs from rat BM, lipid-polymer nanocapsules - SPION-PLGA-PEG	A) Magnetic targeting of cells in 3% agarose phantom. B) Magnetic targeting of cells in a tube (simulated carotid artery, internal diam. 1 mm, external diam. 2 mm).	A) Permanent cylindrical magnet (25*30 mm, B=0.35 T). Exp.: 90 s. B) Two permanent cubic magnets (4 mm, B=0.3 T). Exp.: n/d.	A) Cell displacement in MF in agarose phantom. B) Cell accumulation at vessel wall in MF zone.	(25)
Neutrophils, SPION- gelatin-paclitaxel-E. coli membrane	A) Magnetic targeting of cells in a microfluidic chip in whole blood (flow rate 100-700 µm/s). B) Magnetic targeting of cells in rat aorta with or without chemoattraction. C) Cell migration in MF in Transwell chamber through bEnd.3 cell line layer (blood-brain barrier model) with or without chemoattraction.	A) RMF device (B=0.006-0.018 T, frequency 1-200 Hz). Exp.: n/d. B) RMF device (B=0.015 T, frequency 2 Hz). Exp.: n/d. C) RMF device (B=0,015 T, frequency 2 Hz). Exp.: 3 h.	A) Neutrophil speed in VMP (18 mT, 5 Hz) at blood flow rates of 0, 100, 400 and 700 µm/s: 18.5, 17.6, 13.8 and 11.6 µm/s respectively. B) Avg. speed on vessel surface in RMF: 4 µm/s (vs. 0.17 µm/s with chemotaxis). C) ↑ neutrophil migration across blood-brain barrier in RMF ×3.3 (no chemoattraction) and ×1.7 (with chemoattraction).	(29)

Abbreviations: APS – 3-aminopropyltriethoxysilane; AT – adipose tissue; BM – bone marrow; CCL21 – C-C motif chemokine ligand 21; CCR2 – C-C motif chemokine receptor 2; Cit – citrate; CTLs – cytotoxic T lymphocytes; CXCR4 – C-X-C motif chemokine receptor 4; DMSA – dimercaptosuccinic acid; EPCs – endothelial progenitor cells; ESCs – embryonic stem cells; Exp. – exposition time; FION – ferrimagnetic iron oxide nanocubes; MF – magnetic field; MMP13 – matrix metalloproteinase 13 (collagenase-3); MPIO – microparticles of iron oxide; MMSCs – multipotent mesenchymal stromal cells; n/d – no data; NdFeB – neodymium-iron-boron; PBS – phosphate-buffered saline; PEG – polyethylene glycol; PDA – polydopamine; PGS – polyglycerol sebacate; PLGA – poly(lactic-co-glycolic acid); PLL – poly-L-lysine; PCL – polycaprolactone; PVP – polyvinylpyrrolidone; RMF – rotating magnetic field; SDF-1 – stromal cell-derived factor 1 (CXCL12); SOX9 – SRY-box transcription factor 9; SPION – superparamagnetic iron oxide nanoparticles; T – Tesla (the unit of magnetic flux density); TIMP3 – tissue inhibitor of metalloproteinases 3; TMCs – trabecular meshwork cells; UC – umbilical cord; WJ – Wharton's jelly.
cells; UC – umbilical cord; WJ – Wharton's jelly.

[Downloaded from mjiri.iums.ac.ir on 2026-10-14]

[DOI: 10.47176/mjiri.39.91]